Magnetic Emulation of Microgravity for Earth-Bound Multiphase Catalytic Reactor Studies—Potentialities and Limitations

Faïçal Larachi and Mugurel C. Munteanu
Dept. of Chemical Engineering, Laval University, Québec, Canada, G1V 0A6

DOI 10.1002/aic.11752
Published online March 16, 2009 in Wiley InterScience (www.interscience.wiley.com).

A method is proposed to generate Earth-bound artificial microgravity in a controlled facility capable of emulating lunar/Martian gravity or microgravity for experiments on passive/reactive catalytic multiphase flows. Its applicability was illustrated for trickle beds where flowing gas and liquid experience artificial microgravity inside the bore of a superconducting magnet generating large gradient magnetic fields to compensate for gravity. Artificial gravity is realized by commuting into apparent gravity acceleration the magnetization force at work on common ''chemical engineering'' non-magnetic fluids. The scaling property to be matched and maintained invariant in multiphase systems to achieve magnetic mimicry is phasic mass magnetic susceptibility. Hydrodynamic (liquid holdup, wetting efficiency, pressure drop) as well as catalytic reaction (conversion and selectivity) measurements were obtained. The main finding is a proof that magnetic fields affect reactor outcomes exclusively via hydrodynamic phenomena making them appealing proxies for emulating non-terrene reactor applications. © 2009 American Institute of Chemical Engineers *AIChE J,* 55: 1200–1216, 2009
Keywords: microgravity, magnetic field, mass susceptibility, catalytic reaction, trickle bed

Introduction

Studies of flow/transport/reaction phenomena in hypogravity/microgravity [in short μ-gravity] for space applications are of particular significance for life support systems, e.g., Advanced Life Support,[1–6] Low Earth Orbit,[7] In-situ Resource Utilization[8,9] and Human Exploration & Development Space[5] programs. Of equal importance is the study in μ-gravity of multiphase reactors to understand their behavior in non-terrene conditions in support of long-duration human missions in space.[10,11] For instance, water recovery systems based on packed-bed bioreactors to remove carbon and to convert ammonia to nitrite and nitrate from spacecraft gray wastewater were in the line of sight of NASA's Advanced Life Support Project Plan.[3,4] Lack of accessibility, and cost and complexity constraints for implementing testing platforms and protocols are obvious limitations why μ-gravity data on multiphase reactors remain very scarce. Despite life support research attempts to establish reliable and predictive models that can be used as a basis for design of life support hardware for microgravity applications, e.g., lunar ($0.165g$) and Martian gravity ($0.38g$),[3] a major obstacle in developing adapted multiphase reactor concepts for life support in μ-gravity is an insufficient knowledge concerning the interrelations, once in space, between fluid flows, fluid/fluid interactions and chemical/catalytic reactions.

Following the work by Beaugnon and Tournier[12] on magnetic levitation, strong inhomogeneous magnetic fields generated in superconducting magnets have been used to emulate a variety of phenomena in μ-gravity conditions.[13–16] It was established that strong inhomogeneous magnetic fields allow (non-magnetic) diamagnetic materials to be levitated by counterbalancing their weight. By extension, the ability to influence the behaviors of non-magnetic fluids in multiphase

Correspondence concerning this article should be addressed to Faïçal Larachi faical.larachi@gch.ulaval.ca

reactors by magnetic field emulation represents a scientific challenge as it could provide an additional tool for earth-bound research on μ-gravity. For example, operating multiphase reactors in a magnetically-emulated artificial gravity environment to monitor the course of catalytic reactions in it would be far much simpler than to resort to the currently available tools for microgravity generation. As a matter of fact, magnetic field emulation of artificial gravity could be sustained for days without interruption by means of superconducting magnets. This is unlike in the traditional parabolic aircraft flight campaigns which, apart from being not easily accessible, do not permit tests to lapse more than about 0.5 min in a series of consecutive dives. This could represent an inherent limitation for processes with longer characteristic times such as slow catalytic reactions or vessel residence times in excess of the duration of the μ-gravity operating window. Also, magnetically-assisted μ-gravity on Earth is far much cheaper to achieve as compared to that using μ-gravity carriers such as manned or automated orbital platforms.[1] This would open up new research opportunities for multiphase reactors using magnetically assisted methods to achieve Mars, Moon, or microgravity processing rates on Earth. It seems none has attempted yet *multiphase* reactor experiments with catalytic reactions using strong gradient-magnetic fields for emulating μ-gravity.[17]

In chemical flow processes, fluids are of chief importance while very often they exhibit non-magnetic behavior as assessed from their considerably low *volumetric* magnetic susceptibility values, typically in the range $\pm$ [10^{-6}:10^{-7}]. Flows of such non-magnetic fluids might eventually be magnetically stimulated provided strong gradient-magnetic fields, such as those produced in superconducting magnets, are used. A strong inhomogeneous magnetic field acting on a fluid phase α gives rise to the so-called Kelvin magnetic force density,[18] $\underline{\mathbf{F}}_{M\alpha} = \chi_\alpha/((1 + \chi_\alpha)^2\mu_0)\ \underline{\nabla}\ \underline{\mathbf{B}} \cdot \underline{\mathbf{B}} \approx \chi_\alpha/\mu_0\ \underline{\nabla}\ \underline{\mathbf{B}} \cdot \underline{\mathbf{B}}$, which is a *body* force density and in that sense is analogous to the gravity body force density, $\rho_\alpha\ \underline{\mathbf{g}}$. Gravitational and magnetic forces represent the effects of long-range (or action-at-a-distance) forces and are applied on every molecule of the material content of the volume element. This is unlike the surface forces which are direct-contact or push-pull-shear forces and which are exerted on the elements' surface by the contiguous surroundings.[18,19] Hence, in essence, the main role of the Kelvin magnetic force compared to gravity force is to allow a directional control for mimicking non-terrestrial μ-gravity conditions by artificially compensating the body's weight even to eventually reach a state of weightlessness. This technique has been used to levitate a range of compounds and organisms in ground-based experiments.[12,20–23] It is worthy of notice that the Kelvin force acts upon electrically non-conducting non-magnetic fluids as commonly encountered in chemical engineering. It should not be confused with the Lorentz magnetohydrodynamic force, $\underline{\mathbf{F}}_{L\alpha} = \sigma_\alpha(\underline{\mathbf{E}} + \boldsymbol{v}_\alpha \wedge \underline{\mathbf{B}}) \wedge \underline{\mathbf{B}}$, which concerns electrically conducting fluids such as liquid metals, strong electrolytic solutions and plasmas,[24] that experience magnetic (but not necessarily inhomogeneous) fields.

Application of Kelvin forces to multiphase catalytic reactors is still poorly explored in the literature. In this work, we propose the use of a controlled laboratory facility capable of providing simulated lunar/Martian or microgravity environments for experiments on passive/reactive multiphase flows. We will illustrate its application in the case of a miniature trickle-bed reactor which consists of gas-liquid co-current flows through a fixed bed of inert as well as catalytic particles. The gas and liquid flows could feel μ-gravity in the trickle bed placed inside the atmospheric bore of a superconducting magnet generating large magnetic field strengths and magnetic field gradients to compensate for gravity.

Experimental Setup

Magnet setup

Figure 1a illustrates the experimental setup used to generate an inhomogeneous two-dimensional axisymmetrical ($B_\theta = 0$, $\partial B_\theta/\partial \square = 0$, $\partial \square /\partial\theta = 0$) magnetic induction field $\underline{\mathbf{B}} = (B_r\ 0\ B_z)$ up to 9 Tesla in a superconducting NbTi solenoid magnet system (American Magnetics) placed in *upright* position. To reach the superconducting state, the solenoid temperature is maintained at 4.2 K by immersing it in a (liquid) ^{L}He-containing compartment, itself confined in $^{L}N_2$ and high-vacuum insulation compartments inside a Dewar vessel. The vertically-oriented magnetic field is generated and controlled by changing the current density through the magnetic coil. This is allowed by means of a computerized control system capable of generating, along the bore centerline, *m*aximum (and *m*inimum) *p*eak *p*roduct *g*radients $B_z\partial B_z/\partial z$ of $MPPG_A = +650\ T^2/m$ and $MPPG_A, = -650\ T^2/m$, respectively, at points A and A′. These points are situated 12.5 cm apart from each other (Figure 1b). The accessible cylindrical enclosure inside the atmospheric bore of the magnet is 2.5 cm in diameter and 30 cm in length. However, between points A and A′ lies a region, about 40% of the magnet length, where $B_z\partial B_z/\partial z$ nears zero (Figure 1b) hence disqualifying this area for μ-gravity tests.

Trickle bed setup

A miniature trickle-bed reactor ($L = 4$ cm in length, $D =$ 1.6-cm internal diameter), equipped with non-magnetic inlet and outlet valves, is positioned vertically and adjusted along the symmetry axis inside the atmospheric bore to allow two-phase flow hydrodynamics, mass transfer and reaction tests to be conducted. The region of interest (ROI) in which the trickle bed is placed extends radially between 0 and 0.8 cm and axially between $z = +$ (respectively, –)10 cm and $z = +$ (respectively, $-$)14 cm around A (respectively, A′). The trickle bed is slid in the bore until $MPPG_A$ (or $MPPG_{A'}$) coincides with the center of the bed middle plane (Figure 1a). Typically, 1-mm diameter inert glass beads sandwiching a 10 mm layer of 16–20 mesh (about 0.91 mm) catalytic particles constitute the fixed-bed inventory for conducting catalytic hydrogenation of liquid-dissolved reactants in the recycle-mode with respect to liquid phase. Thinner catalyst beds would have, on the one hand, necessitated excessively long reaction times before acceptable conversions could have been attained. Due to the non-linear space dependence of the $B_z\partial B_z/\partial z$ function (Figure 1b), taller beds, on the other hand, would have precluded delineating a region in the magnet bore where nearly constant apparent gravity force could have been assumed. Therefore, the catalyst bed thickness represented a compromise between the finite evaporation

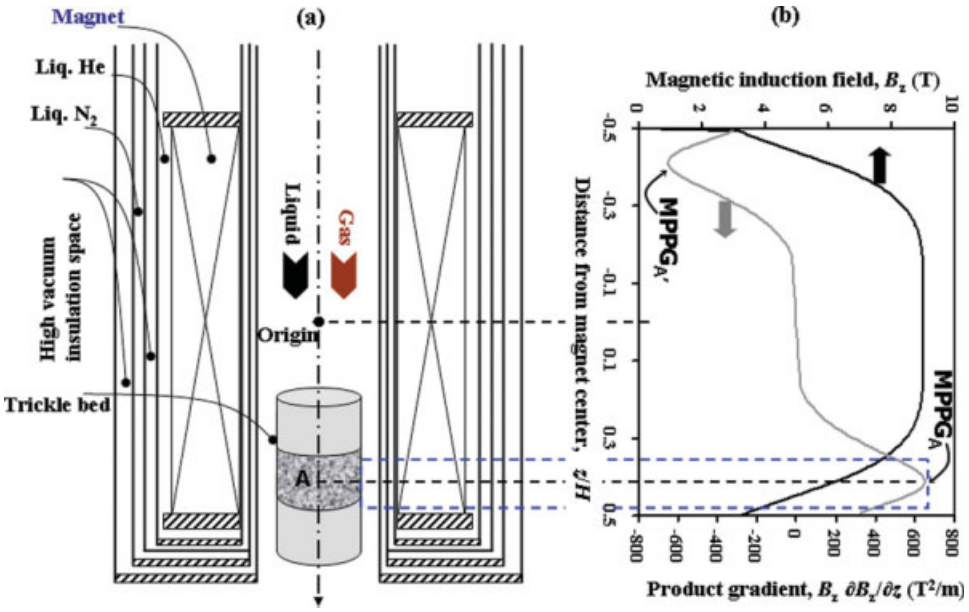

Figure 1. Superconducting 9 T magnet setup with trickle bed inside atmospheric magnet bore (a) and centerline ($r = 0$) axial distributions of magnetic field, B_z, and magnetic induction × magnetic induction gradient, $B_z \partial B_z/\partial z$, at 9 T (b).

[Color figure can be viewed in the online issue, which is available at www.interscience.wiley.com.]

time of ^{L}He in the Dewar, the degree of spatial homogeneity of μ-gravity and the measurements of meaningful liquid reactant conversions. The magnetic field intensity inside and outside of the bore was measured using a Hall effect Gaußmeter (GM-700, Cryogenics). The magnetic susceptibilities of the liquid solutions involved in the experiments were determined using a MicroMag^{TM} 2900 alternating gradient magnetometer (Princeton Measurements Corporation).

Catalytic reactions and analytical procedures

The first test reaction chosen for this study was hydrogenation of α-methylstyrene (αMS) to cumene:

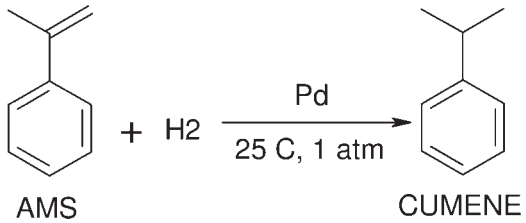

This reaction has been studied extensively by a number of investigators,[25–29] and is known to proceed with a noticeable rate even at ambient temperature and hydrogen pressure. It is frequently used to decipher mass transfer limitations with regard to catalyst wetting efficiency in three-phase catalytic reactors. As wetting efficiency in partially wetted trickle flow regime is related to conversion, in particular in liquid-reactant limited regime, analysis of the catalytic reaction outcome under magnetic field will be insightful. In the literature, it is often admitted that hydrogenation of αMS is zeroth-order with respect to αMS and a first-order with respect to H_2.[25] The boiling points of αMS (164°C), cumene (152°C) and styrene (internal standard, 146°C) are all relatively high and the reaction mixture is easily analyzed using standard gas chromatography.

Reagent grade (99% purity) α-methylstyrene (Sigma-Aldrich) containing 15 ppm of *t*-butylcatechol as polymerization inhibitor was dissolved in kerosene solvent. The polymerization inhibitor was eliminated by contacting αMS with γ-alumina for several hours. It was found that the water traces strongly decrease the reaction rate.[29] To avoid that the solution was passed through a 10A molecular sieve to reduce as much as possible the amount of water. The catalyst, 1 %wt Pd/ polyethyleneimine/silica (Royer Palladium catalyst) purchased from GFS Chemicals, was activated before reaction under H_2 stream for 4 h at 40°C. A volume of 50 mL 0.16 M αMS/kerosene solution was loaded in a liquid reservoir and recirculated long enough at high throughput using a peristaltic pump to ensure pre-wetting of the catalyst. The reaction was initiated by flowing H_2 through the reactor at prescribed flow rates. Samples were taken from the liquid phase at regular intervals and analyzed on a Hewlett-Packard 5890 Series II gas chromatograph using a 30 m × 32 mm × 25 μm model DB-5MS packed column. Peak areas of the compound of interest were normalized relative to styrene (internal standard) and converted to concentration via calibration curves generated experimentally following the internal standard technique.

The second reaction system selected for the experiment was the catalytic hydrogenation of phenylacetylene (Reagent grade, 99% purity from Sigma-Aldrich). The experiment involves hydrogenation of phenylacetylene (PA) to styrene (S) and ethylbenzene (EB) over Pt 1% on polyethyleneimine/SiO_2 (purchased from Alpha Aesar). A volume of 50 mL 0.15 M PA/kerosene/*n*-decane solution was introduced

to the liquid reservoir. The reaction scheme consists of two consecutive steps in parallel with a single step directly to the final hydrogenation product:

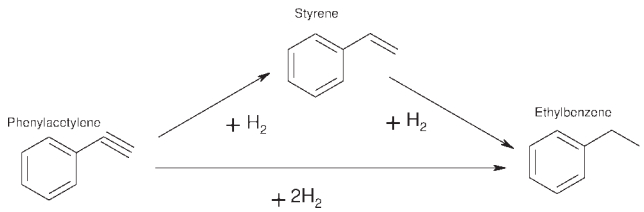

This triangular reaction scheme presents a simple selectivity tool that will allow to probe the effects of magnetically-emulated μ-gravity owing to the relatively soft operating conditions in which it can be conducted.[30–34] The boiling points for PA (144°C), S, EB (136°C) and *n*-decane (as internal standard) are all reasonably high, and the reaction mixture is analyzed using gas chromatography. It was not possible to use the same internal standard as before (styrene), because styrene is one of the reaction products. The rest of the experimental procedure is similar to that with αMS.

Liquid holdup, pressure gradient, and wetting efficiency determinations

Liquid holdup was determined by the weighing method with the reactor filled with 1-mm diameter glass beads (bed porosity = 0.37). The reactor was placed inside the coil bore and experiments were run at different fluid velocities and magnetic field levels. The liquid phase was first passed through the reactor for a period of time at high velocity to achieve fully pre-wetted bed. Subsequently, the liquid velocity was set at the desired value and the gas phase was fed to the reactor via a pressure regulator. As soon as steady state was attained, both inlet and outlet valves were closed instantaneously. The reactor was weighed and the external liquid holdup was estimated from the weight difference between wet and dry reactor volume. A differential pressure transducer (C 9551, Comark) was used to measure simultaneously the two-pressure drop across the bed. The experiments were carried out both in down-flow and in upflow modes.

Wetting efficiency experiments were performed on the same bed using a colorimetric method inspired from the work of Lazzaroni et al.[35] The glass beads were colored before the experiment with a crystal violet solution of known concentration. The miniature reactor with the colored beads inside was inserted into the solenoid bore. Depending on liquid and gas flow throughputs, the particles color was more or less washed out by the sweeping liquid. The solution transmittance was measured at each liquid flow rate change using a spectrophotometer (Spectronic 20, Milton Roy Company) after steady-state solution transmittance was attained depending on imposed flow rates. The final concentration when no more color was left on glass beads was considered as 100% when the glass beads were fully washed and wetting was total. The wetting efficiency was calculated as the ratio between the intermediate and final concentrations in the liquid phase for both enabled and disabled magnetic field modalities.

How to Achieve Magnetic Mimicry of μ-Gravity in Trickle Bed?

To assess the relative importance of gravity vs. magnetic forces, a gravitational amplification factor, γ_α, for any α-phase of the two-phase flow is defined whereby $F_{M\alpha}$ can be commuted into apparent gravity acceleration. As shall be later discussed, assuming the main direction of magnetic-field *gradient* parallel to the gravitational field, one can define γ_α as:

$$\gamma_\alpha = \frac{\rho_\alpha g + F_{M\alpha}}{\rho_\alpha g} = 1 + \frac{\chi_\alpha}{\rho_\alpha g \mu_0} B_z \frac{\partial B_z}{\partial z} \tag{1}$$

In Eq. 1, B_z = vertical component of the magnetic flux density, $F_{M\alpha}$ = vertical component of the magnetic force density in α-phase, g = Earth gravity acceleration, χ_α = α-phase volumetric magnetic susceptibility, μ_0 = absolute magnetic permeability of vacuum, ρ_α = α-phase density, and $\chi_\alpha/\rho_\alpha = \hat{\chi}_\alpha$ = α-phase mass magnetic susceptibility.

Depending on the signs of χ_α ($\chi_\alpha > 0$ for paramagnetic and $\chi_\alpha < 0$ for diamagnetic) and of the gradient of magnetic flux density, four cases arise for the α-phase: (a) $\gamma_\alpha > 1$ macrogravity (or hypergravity); (b) $0 < \gamma_\alpha < 1$ microgravity or hypogravity; (c) $\gamma_\alpha = 0$ levitation; (d) $\gamma_\alpha < 0$ if the magnetic force, oriented anti-parallel to the weight, outweighs this latter.

Two conditions must be met to accomplish magnetic mimicry of μ-gravity in both gas and liquid:

[C^1] Eq. 1 indicates that for γ_l and γ_g to be equal, it suffices to fulfill mass susceptibility matching between the gas (g) and liquid (l) phases such that:

$$\hat{\chi}_g \approx \hat{\chi}_l \quad \Rightarrow \quad \gamma_g \approx \gamma_l \tag{2}$$

As it appears from Eq. 2, the feasible combinations for achieving identical μ-gravity "feelings" for gas-liquid flows are: paramagnetic gas–paramagnetic liquid or diamagnetic gas–diamagnetic liquid.

[C^2] There has to be a finite (and continuous) domain V within the ROI for which:

$$\gamma_g\big|_{V \subset ROI} \approx \gamma_l\big|_{V \subset ROI} \approx \text{constant} \tag{3}$$

Equation 3 signifies that γ_l and γ_g must also take a common *constant* value over a finite volume V so that nearly the same apparent gravity would be felt by both fluids. This volume shall not be too slim to compromise experimental feasibility as explained in the Experimental Setup section earlier.

μ-Gravity using paramagnetic gas and liquid

Air-water solutions concern the first case. The value of (paramagnetic) air mass magnetic susceptibility at ambient temperature and atmospheric pressure is $3.15 \cdot 10^{-7}$ m^3/kg.[36] A straightforward way for turning (diamagnetic) water into a paramagnetic solution is through dissolving salts of paramagnetic metal cations, an example of which could be divalent manganese chloride. The salt concentration set to achieve a mass magnetic susceptibility of the aqueous solution equal, at ambient temperature and atmospheric pressure, to that of air was 34.5% w/w of $MnCl_2$ tetra-hydrate. The measured density and kinematic viscosity of this solution were,

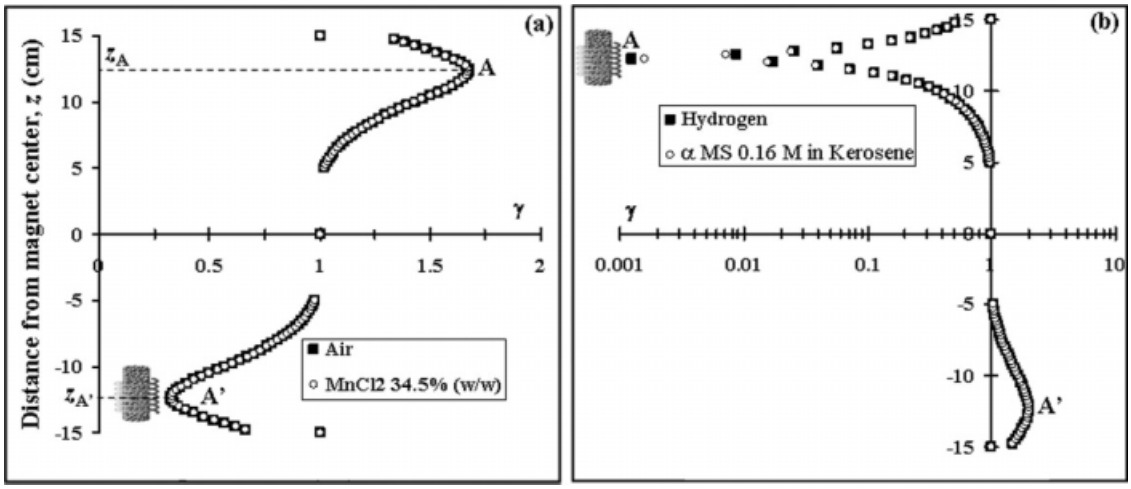

Figure 2. Centerline ($r = 0$) gravitational amplification factor for (a) air/$MnCl_2$ 34.5% (w/w) : maximum $B_z = 0.36$ T, $MPPG_{A'} = -26.3$ T^2/m (b) H_2/αMS 0.16 M + kerosene : maximum $B_z = 6.76$ T, $MPPG_A = 488.6$ T^2/m.

respectively, 1346 kg/m^3 and $2.23 \cdot 10^{-6}$·m^2/s. This makes this system relatively far from the academic air/water test system to refrain from drawing analogies between the two systems in artificial gravity conditions.

The per-phase magnetic forces, generated by the magnet, act on air and on the salt solution in a collinear manner. The vertical axis being oriented downwards (Figure 1a), they point upwardly (respectively, downwardly) when $B_z \partial B_z/\partial z < 0$ (respectively, > 0), i.e., subtractive (respectively, additive) with respect to the per-phase gravity forces to cause μ-gravity (respectively, macrogravity). By applying a maximum magnetic field strength of 0.36 T, $B_z \partial B_z/\partial z$ is set to span the interval [−26.3:26.3 T^2/m] over the enclosure length of the magnet. The corresponding γ_l and γ_g span the range [0.32:1.67] while **[C^1]** is satisfied as Figure 2a shows from their evolution along the bore centerline.

The center of mass of the trickle bed coincides with $MPPG_{A'} = \cdot 26.33$ T^2/m. This results in bed-averaged amplification factors of, respectively, 0.417 for air and 0.420 for the salt solution. These μ-gravity conditions are close to those encountered on Mars planet and correspond to magnetic body force densities of $F_{Ml} = -8875$ N/m^3 for the manganese chloride solution and $F_{Mg} = -8$ N/m^3 for air. Note that the solution electrical conductivity, estimated to be about 40 $\Omega^{-1} \cdot m^{-1}$,[37] gives rise to Lorentz force densities varying over the reactor bed length, L, between $1.2 \cdot 10^{-3}$ and $5.7 \cdot 10^{-3}$ N/m^3. As can be seen, the influence of the Lorentz force densities can safely be ignored with respect to the Kelvin magnetic force densities in action.

μ-Gravity using diamagnetic gas and liquid

The second selected gas-liquid system consists of combination of diamagnetic gas and liquid which must also fulfill **[C^1]**. Such systems are representative of catalytic hydrogenation reactions involving dissolved reactants in organic liquids. Catalytic hydrogenations of α-methylstyrene (αMS) or phenylacetylene (PA) were selected as model reactions for the experimental tests. Pure hydrogen is diamagnetic and has a mass magnetic susceptibility of $-2.52 \cdot 10^{-8}$ m^3/kg at 20°C and atmospheric pressure. The measured mass magnetic susceptibility of pure αMS value is $-8.50 \cdot 10^{-9}$ m^3/kg. Therefore, αMS was mixed with several solvents in an attempt to select solutions achieving $\hat{\chi}_g \approx \hat{\chi}_l \approx -2.52 \cdot 10^{-8}$ m^3/kg. Kerosene, whose measured mass magnetic susceptibility is $-2.56 \cdot 10^{-8}$ m^3/kg, was found to be an appropriate hosting liquid. Figure 2b illustrates the centerline γ_l and γ_g profiles along the magnet bore determined for 0.16 M αMS/kerosene ($\rho_l = 802.6$ kg/m^3) and pure gaseous hydrogen phases. For a 6.76 T maximum magnetic field strength, the product $B_z \partial B_z/\partial z$ varies over the open bore length in the range [−488.6:488.6 T^2/m]. This yields gas and liquid gravitational amplification factors, γ_l and γ_g, to evolve in the range [0.001:1.99] while satisfying **[C^1]**. By sliding the trickle bed to adjust its middle plane on $MPPG_A = +488.6$ T^2/m, the gas and liquid phases would feel $\gamma_l \approx \gamma_g \approx 10^{-3}$ at the elevation z_A (Figure 2b). A similar methodology was followed in the case of the 0.15 M PA/kerosene/H_2 system.

Factors Affecting the Degree of Homogeneity of μ-Gravity

The influence of strong magnetic fields just described above could hide unsuspected phenomena, related to the nature of multiphase systems, other than the hydrodynamic force effects highlighted by Eq. 1. It is hence important to understand how $\hat{\chi}_\alpha$ and $\underline{\mathbf{B}}$ can modify γ_α inside the catalyst bed domain. This is tantamount to identify the various factors, and then to quantify their incidence, to judge of their extent at demising the validity of the concept of magnetic mimicry of μ-gravity in multiphase systems. Trickle beds involve several physicochemical factors associated with two-phase flows and catalytic reactions, such as thermodynamic equilibria (gas dissolution, solvent evaporation), mass transfer (concentration gradients across interfaces), conversion (species production/consumption) and heat effects (temperature gradients). Therefore, in addition to restrictions inherent, as shown above, to the spatial non-homogeneity of $\underline{\mathbf{B}}$ itself, all these factors may also influence or be influenced, whether directly or indirectly, by the imposed magnetic field. In

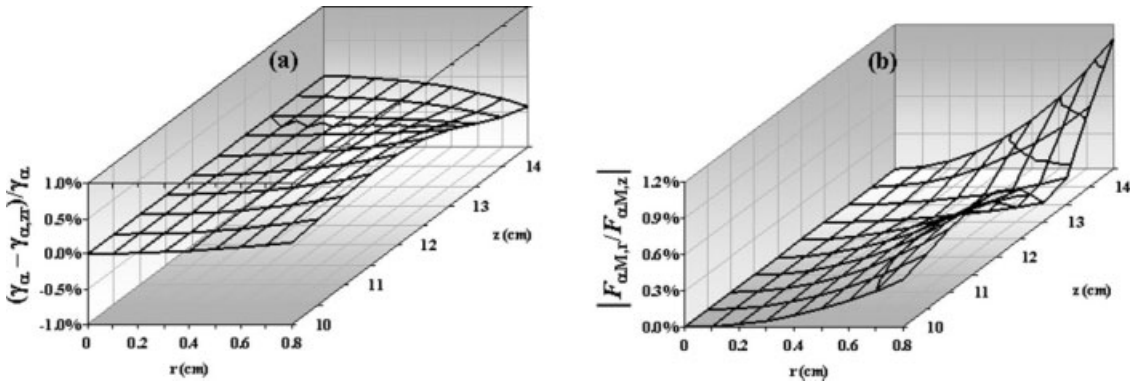

Figure 3. Mapping of (a) relative residuals of γ_l or γ_g computed as Eq.1 and as $\gamma_{\alpha,zr} = 1+\chi_\alpha/\rho_\alpha g\mu_0$ ($B_z\partial B_z/\partial z + B_r\partial B_r/\partial z$) (b) radial-to-axial ratio of magnetic force components.

H_2/αMS 0.16 M + kerosene in the trickle bed ROI: maximum $B_z = 8.25$ T.

return, this may translate in uncontrollable variations of the mass magnetic susceptibilities of gas and liquid during their journey inside the reactor which could result in violation of **[C^1]** and/or **[C^2]**.

Axial vs. radial/azimuthal kelvin magnetic force components

Due to the solenoidal nature of magnetic fields, an inhomogeneous magnetic field along z axis implies, similarly to B_z (Figure 1), a space-dependent B_r which, in axisymmetrical fields, could also contribute to the *vertical* body force effect via the term $B_r\partial B_r/\partial z$. *Stricto sensu*, therefore, the vertical component of the magnetic force, $F_{M\alpha,z}$, and the gravitational amplification factor, $\gamma_{\alpha,zr}$, should write, respectively, as:

$$F_{\alpha M,z} = \frac{\chi_\alpha}{\mu_0}\left(B_z\frac{\partial B_z}{\partial z} + B_r\frac{\partial B_r}{\partial z}\right) \tag{4}$$

$$\gamma_{\alpha,zr} = 1 + \frac{\chi_\alpha}{\rho_\alpha g\mu_0}\left(B_z\frac{\partial B_z}{\partial z} + B_r\frac{\partial B_r}{\partial z}\right) \tag{5}$$

Exemplified in the case of 0.16 M αMS+kerosene/H_2 system, Figure 3a confirms that the truncated form Eq. 1 still approximates very well the values of γ_α given that the relative residuals with respect to Eq. 5 seldom exceed 0.5%.

Furthermore, to mimic as closely as possible μ-gravity, the magnetic azimuthal and radial force components must remain marginal with respect to their axial component counterpart:

$$|F_{\alpha M,r}| = \left|\frac{\chi_\alpha}{\mu_0}\left(B_z\frac{\partial B_z}{\partial r} + B_r\frac{\partial B_r}{\partial r}\right)\right| \ll |F_{\alpha M,z}| \tag{6}$$

$$F_{\alpha M,\theta} = 0 \tag{7}$$

Figure 3b confirms for the same system that the radial magnetic force component computed according to Eq. 6 never exceeds 1.2% of its axial counterpart (Eq. 4) within the trickle bed ROI. This confirms that except the direction of net fluid flow, the magnetic body force effects in the radial and azimuthal (Eq. 7) directions can be safely neglected. Similar conclusions can be drawn also in the case of the paramagnetic system. Henceforth, only the effects of the vertical component of the magnetic flux density will be accounted for.

Effect of spatial distribution of magnetic field

Referring to **[C^2]** above and as illustrated in Figure 1b, it must be emphasized that due to constraints in solenoid design $B_z\partial B_z/\partial z$ can be assumed roughly constant only over restricted volumes in the magnet enclosure. For symmetry reasons, such volumes where μ-gravity prevails are centered on $MPPG_{A'}$ for paramagnetic (Figure 2a) or $MPPG_A$ for diamagnetic systems (Figure 2b). Therefore, it is important to establish the domain *size* of V (ROI wherein Eq. 3 can be accepted as a valid approximation.

To evaluate the extent of radial homogeneity of γ_α, the discrepancy between $\gamma_\alpha(r = 0,z)$ and a sliding average $\gamma_R(z)$, Eq. 8, was computed. The sliding average was expanded circumferentially outwards as a function of the interval length (or radius) R until the bed wall $R = D/2$ was reached:

$$\gamma_R(z) = \frac{1}{\pi R^2}\int_0^R 2\pi r\gamma_\alpha(r,z)\mathrm{d}r \qquad R = 0\ldots D/2 \tag{8}$$

Similarly, the extent of axial homogeneity of γ_α was assessed by comparing the centerline artificial gravity factor values $\gamma_\alpha(0,z_A)$ at $MPPG_A$ (or $MPPG_{A'}$) with respect to the sliding volume-average γ_Z expanding axially around z_A with interval lengths Z until $\pm Z = \pm L/2$:

$$\gamma_z = \frac{1}{2Z}\frac{4}{\pi D^2}\int_{-z}^{+z}\int_0^{D/2} 2\pi r\gamma_\alpha(r,z)\mathrm{d}r\mathrm{d}z \quad Z = 0\ldots L/2 \tag{9}$$

Figure 4a, exemplifying the 0.16 M αMS + kerosene/H_2 system, shows the degree of radial homogeneity, expressed as residuals of $|\gamma_\alpha(0,z) - \gamma_R(z)|/\gamma_\alpha(0,z)$ for three axial cuts in the trickle bed ROI: entrance ($z = 100$ mm), near point A ($z = 125$ mm) and exit ($z = 140$ mm). At $MPPG_A$ $\gamma_g \approx \gamma_l \approx 10^{-3}$. The local γ_α values do not change significantly as revealed by the relative differences, typically less than 1% irrespective of z position, between centerline $\gamma_\alpha(0,z)$ and

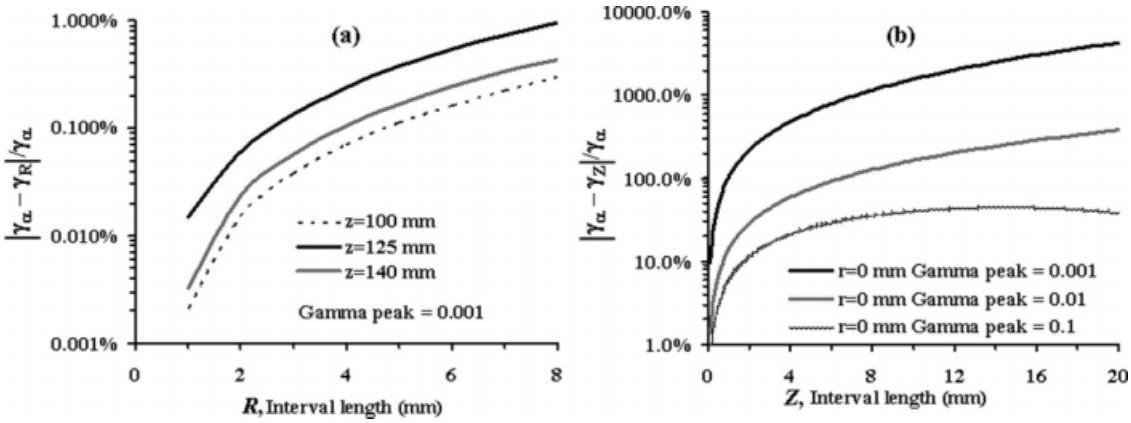

Figure 4. Homogeneity of gravitational amplification factor as a function of interval length for αMS/kerosene-H_2 system.

(a) radially at $z = 100$, 125, and 140 mm, $MPPG_A = 488.6$ T^2/m, maximum $B_z = 6.76$ T, peak $\gamma_\alpha = 10^{-3}$ (b) axially along bore centerline : peak $\gamma_\alpha = 10^{-3}$ ($MPPG_A = 488.6$ T^2/m, maximum $B_z = 6.76$ T), peak $\gamma_\alpha = 10^{-2}$ ($MPPG_A = 485$ T^2/m, maximum $B_z = 6.72$ T), and peak $\gamma_\alpha = 10^{-1}$ ($MPPG_A = 440$ T^2/m, maximum $B_z = 6.1$ T).

averaged $\gamma_R(z)$. Hence, radial homogeneity of the gravitational amplification factor is virtually verified everywhere within ROI. Assigning peak $\gamma_\alpha = 10^{-2}$ and 10^{-1} at $MPPG_A$ (not shown) led to radial homogeneity within 10%.

Similarly, Figure 4b shows the degree of axial homogeneity, expressed as $|\gamma_\alpha(0,z_A) - \gamma_Z|/\gamma_\alpha(0,z_A)$ for successive peak values $\gamma_\alpha = 10^{-3}$, 10^{-2}, and 10^{-1}. It can be seen that the approximation of homogeneity in axial direction is more stringent and is achievable only within increasingly slimmer volumes as lower peak γ_α values are to be imposed. Hence, gas and liquid flows across 10 mm catalyst height would feel homogeneous μ-gravity environments within 20% around $\gamma_\alpha = 10^{-1}$ and 50% around $\gamma_\alpha = 10^{-2}$. Similar conclusions are drawn also in the case of the paramagnetic system. It appears difficult to achieve acceptable μ-gravity conditions below 10^{-2} for 10-mm catalyst slice. For instance, a catalyst layer as thin as 0.5 mm would have been required to attain $\gamma_\alpha = 10^{-3}$ within 50% error which was not feasible considering our study's constraints as explained earlier.

Effect of gas solubility, solvent evaporation, and diffusion: H_2-kerosene system

The thermodynamics of mixtures subject to magnetic fields can differ from the one in conventional magnetic field-free conditions.[38] As an illustration, the incidence of magnetic fields on gas dissolution and solvent evaporation is analyzed for the binary system H_2 (1)–n-C_{14} (2) at 1 atm and 298 K in which normal tetradecane was used as kerosene proxy. Thermodynamic equilibrium under magnetic fields requires equality for species one and two of their respective magneto-chemical fugacities[38] in gas and liquid:

$$f_i^l(T,P,\mathbf{x})\exp-\frac{B^2}{2\mu_0 RT}\left(\bar{v}_i^l\chi_i^l+\chi_j^l x_j\frac{\partial\bar{v}_j^l}{\partial x_i}+\chi_i^l x_i\frac{\partial\bar{v}_i^l}{\partial x_i}\right)$$
$$=f_i^g(T,P,\mathbf{y})\exp-\frac{B^2}{2\mu_0 RT}\left(\bar{v}_i^g\chi_i^g+\chi_j^g y_j\frac{\partial\bar{v}_j^g}{\partial y_i}+\chi_i^g y_i\frac{\partial\bar{v}_i^g}{\partial y_i}\right) \quad (10)$$

In which $f_i^l(T,P,\mathbf{x})$ and $f_i^g(T,P,\mathbf{y})$ are, respectively, the i-species liquid and gas fugacities at equilibrium T and P without magnetic field. Similarly, $\chi_{i,j}^l$ and $\chi_{i,j}^g$, and $\bar{v}_{i,j}^l$ and $\bar{v}_{i,j}^g$ are, respectively, the i- and j-species liquid and gas volumetric susceptibilities and partial molar volumes. The exponential term, referred to as a Poynting magnetic correction, accounts for inflating (respectively, deflating) the fugacity of diamagnetic (respectively, paramagnetic) species under a magnetic field. The estimation methods used to evaluate the volumetric magnetic susceptibilities in gas and liquid state of H_2 and hydrocarbon, and their corresponding partial molar volumes are described in Appendix A.

The derivative terms $\partial\bar{v}_{i,j}^l/\partial x_i$ in Eq. 10 are omitted assuming that H_2 remains, as in the case of $B = 0$, sparingly soluble in the liquid at ambient conditions. Deviations of hydrogen and hydrocarbon equilibrium mole fractions in gas (y_1, y_2) and liquid (x_1, x_2) under magnetic field with respect to their equilibrium composition alter ego without magnetic field (y_1^o,y_2^o) and (x_1^o,x_2^o) can be estimated using the magnetically-modified versions of Raoult's and Henry's laws for hydrocarbon and H_2, respectively, as well as the ideal gas law:

$$x_1 K_H\exp-\frac{B^2\bar{v}_1^l\chi_1^l}{2\mu_0 RT}=y_1 P\exp-\frac{B^2\chi_1^g}{2P} \quad (11)$$

$$x_2 P_2^v\exp-\frac{B^2\bar{v}_2^l\chi_2^l}{2\mu_0 RT}=y_2 P\exp-\frac{B^2\chi_2^g}{2P} \quad (12)$$

$$x_1+x_2=1 \quad (13)$$

$$y_1+y_2=1 \quad (14)$$

The base case can be retrieved by disabling the magnetic field in Eqs. 11–14 to estimate (y_1^o,y_2^o) and (x_1^o,x_2^o).[42] Figure 5 illustrates the relative deviations, with respect to $B = 0$ case, in mole fractions of dissolved H_2 in liquid hydrocarbon and of hydrocarbon saturated vapor as a function of applied magnetic field. Clearly, though increasing magnetic induction levels has a tendency to imperceptibly drive up hydrocarbon

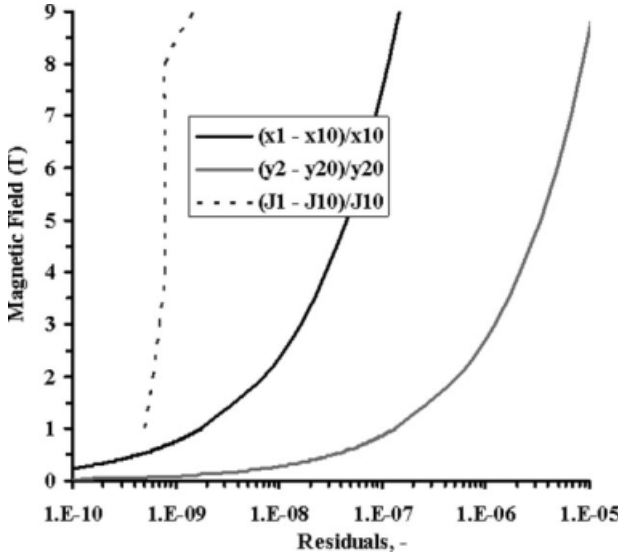

Figure 5. Influence of applied magnetic field on H_2/kerosene VLE and enhanced hydrogen diffusion flux at T = 298 K and P =1 atm assessed in terms of deviations with respect to B = 0 case of H_2 solubility in liquid kerosene, kerosene saturated vapor pressure in gaseous hydrogen, and hydrogen diffusion in kerosene liquid film.

In the case of flux calculations a linear gradient magnetic field is assumed.

evaporation and hydrogen dissolution as well, it can be concluded that the thermodynamic equilibrium is barely influenced by magnetic induction levels up to about 10 T. Classical Raoult's and Henry's laws are sufficient for quantifying these equilibria.

As a matter of fact, during the mass transfer process of kerosene vaporizing and hydrogen dissolving, concentration gradients establish back and forth across the interface before equilibrium is attained. Hence a further worth-assessing question is in what extent the magnetic field strength could afflict the species mass transfer fluxes? To describe diffusion subject to magnetic fields use is made of the generalized driving force and magneto-chemical potentials to express the mole flux[43]:

$$J_i = -\frac{D_i C_i}{RT}\frac{d\bar{\mu}_i}{dz} \tag{15}$$

where J_i, D_i and C_i are, respectively, the i-species total mole flux, diffusion coefficient and concentration, and $\bar{\mu}_i$ is the magneto-chemical potential. This latter could be expressed in terms of the component fugacity defined above. For instance in the liquid phase assuming isothermal diffusion, and after replacing magnetic-field free fugacity, $f_i^l(T,P,\mathbf{x})$, with hydrogen concentration, C_1^o, corresponding to $B = 0$ case, one can rewrite Eq. 15 as follows:

$$J_1 = -D_1 C_1\left(\frac{d\ln C_1^o}{dz} - \frac{\bar{v}_l^l \chi_1^l}{\mu_0 RT} B(z)\frac{dB(z)}{dz}\right) \tag{16}$$

When $B = 0$, Eq. 16 simplifies to:

$$J_1^o = -D_1 C_1^o \frac{d\ln C_1^o}{dz} \tag{17}$$

We define the flux deviation due to the magnetic field by combining Eqs. 16 and 17:

$$\frac{J_1 - J_1^0}{J_1^0} = \frac{C_1}{C_1^0}\left(1 - \frac{\bar{v}_1^l \chi_1^l}{\mu_0 RT} B(z)\frac{dB(z)}{dz}\frac{dz}{d\ln C_1^0}\right) - 1 \tag{18}$$

A hydrogen mass balance equation can be solved in the liquid diffusional film using H_2 interfacial concentration given by Eqs. 11–14. Figure 5 illustrates the H_2 flux deviations as a function of magnetic field level using Eq. 18. Despite we have assumed unrealistically high negative gradient magnetic field of 630 T^2/m across the diffusional film, hydrogen flux changes were virtually indifferent to the applied magnetic. Similar conclusions can be arrived at in the case of kerosene in the gas phase.

The above calculations indicate that the thermodynamics and mass transport as if the magnetic field were absent are still very good approximations.

Though the vapor pressure of kerosene in the gaseous phase is about 131 Pa in ambient conditions, it nevertheless contributes for a kerosene mass fraction of about 10% when H_2 matches up to 1 atm. Therefore, small discrepancies in mass magnetic susceptibilities implied by kerosene evaporation may noticeably alter the values of γ_g (estimated via Eq. 1) especially when the most severe μ-gravity conditions are approached. Similarly, typical saturated mole fraction of dissolved hydrogen in kerosene amounts to 0.031%. This is tantamount to 3.6 ppm of hydrogen mass fraction and would affect at the worst the sixth digit of liquid kerosene mass magnetic susceptibility. Unlike the gas phase, compositional changes of mass magnetic susceptibility due to H_2 dissolution in the liquid phase can safely be ignored.

In the next development, gaseous hydrogen will be considered as being mixed with kerosene vapor by assuming first saturated vapor and then kerosene evaporation proceeding at a finite rate along the trickle bed. A mixture mass magnetic susceptibility is estimated and the gas-side gravitational amplification factor, γ_g, is evaluated and compared with the gravitational amplification factor, γ_{H2}, for an uncontaminated hydrogen gaseous stream.

The mixture mass magnetic susceptibility, $\hat{\chi}_g$, is barycentric in the mass fraction scale of the mass magnetic susceptibilities of its constituents[44,45]:

$$\hat{\chi}_g = w_1 \hat{\chi}_1^g + w_2 \hat{\chi}_2^g \tag{19}$$

In Eq. 19, w_1 and w_2 are the hydrogen and kerosene mass fractions in the gas phase.

Figure 6 shows the centerline axial profiles inside the magnet bore of the relative deviations between γ_{H2} (uncontaminated hydrogen stream) and γ_g for a kerosene-saturated hydrogen gas (Figure 6a) as well as for a mass-transfer controlled kerosene evaporation (Figure 6b). In the latter case, plug flow in the gas phase was assumed and where the volumetric gas-side mass transfer coefficient, $k_g a$, could be approximated using literature correlations.[46–49] It was estimated that $k_g a$ evolves in the range (0.52−1.45) s^{-1} for the

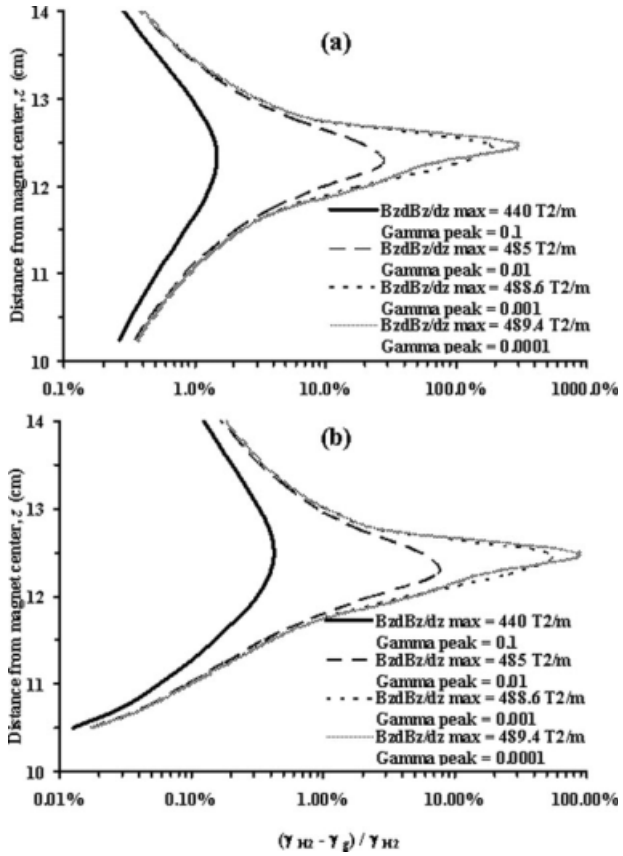

Figure 6. Axial deviations caused by kerosene vapor pressure on local gravitational amplification factor, γ_g along bore centerline at different magnetic fields: (a) kerosene saturated vapor, (b) partially evaporated kerosene pressure computed using Yaïci et al.[46] $k_g a$ correlation for u_l = 0.9 mm/s and u_g = 3.7 cm/s (B_{max} = 6.09 T and $MPPG_A$ = 440 T^2/m : peak $\gamma_g = 10^{-1}$; B_{max} = 6.72 T and $MPPG_A$ = 485 T^2/m : peak $\gamma_g = 10^{-2}$; B_{max} = 6.77 T and $MPPG_A$ = 488.6 T^2/m : peak $\gamma_g = 10^{-3}$; B_{max} = 6.78 T and $MPPG_A$ = 489.4 T^2/m : peak $\gamma_g = 10^{-4}$).

experimental liquid and gas superficial velocities covered in the present study. The results in Figure 6b correspond to u_l = 0.9 mm/s and u_g = 3.7 cm/s for which $k_g a$ takes the lower limit value, i.e., 0.52 s^{-1}. This lower limit together with the saturated kerosene gas phase would set, respectively, the minimum and maximum errors on neglecting solvent evaporation if the magnetic field level is set based on the mass magnetic susceptibility of uncontaminated H_2 gas phase.

The gravitational amplification factors are computed using Eq. 1 for peak gradients of 440 T^2/m whereby $\gamma_{H2} = 10^{-1}$, 485 T^2/m whereby $\gamma_{H2} = 10^{-2}$, 488.6 T^2/m whereby $\gamma_{H2} = 10^{-3}$, and 489.4 T^2/m whereby $\gamma_{H2} = 10^{-4}$. It is in the neighborhood of $MPPG_A$ (or $MPPG_{A'}$) that the deviations would inflate the most due to their lower γ values. As summarized in Table 1, had solvent evaporation been neglected it would have inflicted errors on peak γ at $MPPG_A$, on the γ values averaged over the 1 cm high catalyst layer and on the γ values averaged over the total bed height of 4 cm. Table 1 indicates, especially at deeper microgravity levels (i.e., $\gamma = 10^{-3}$, 10^{-4}) where very high deviations occur, that gas must be preventively pre-saturated with solvent vapor prior to applying condition **[C^1]**. However, down to $\gamma = 10^{-2}$, ignoring corrections about kerosene evaporation and kerosene mass susceptibility remains tolerable. For instance, the errors around $\gamma = 10^{-2}$ over the 1-cm high catalyst layer would have been bracketed between 4.5 and 16.2% at 485 T^2/m (Table 1).

Temperature and conversion effects of catalytic reaction

Until now we were concerned with magnetic field effects in passive systems without reaction taking place in the catalyst bed. Let us now analyze how catalytic reactions going on in the reactor would affect the validity of **[C^1]** and **[C^2]**: (i) temperature changes altering due to (exo)/endothermic effects both gas and liquid magnetic susceptibilities, (ii) species distribution, due to chemical conversion, affecting especially the mixture mass magnetic susceptibility of the liquid phase.

For paramagnetic substances, the volumetric magnetic susceptibility obeys Curie's law ($\chi \sim T^{-1}$).[50] For narrow-ranging temperature variations, the 1/T law is also a good approximation of the mass magnetic susceptibility of paramagnetic liquids ($\hat{\chi}_l \sim T^{-1}$). Because of the density reciprocal dependence, mass magnetic susceptibility of paramagnetic gases at moderate pressures is of the form $\hat{\chi}_g \sim T^0$. Diamagnetic substances are characterized by temperature-indifferent volumetric magnetic susceptibilities ($\chi \sim T^0$).[50] As far as narrow-ranging temperature variations are concerned, this translates in temperature-indifferent liquid mass magnetic susceptibility ($\hat{\chi}_l \sim T^0$); whereas gas mass magnetic susceptibility at moderate pressures is proportional to temperature ($\hat{\chi}_g \sim T$).

As catalytic hydrogenations are exothermic and as far as gas diamagnetic–liquid diamagnetic reacting systems, as those under current study, are concerned, temperature changes are anticipated to alter $\hat{\chi}_g$ and thus γ_g (refer to the previous discussion on kerosene evaporation). From the liquid side, conversely, compositional changes and not temperature ($\hat{\chi}_l \sim T^0$) are thought to disturb γ_l invariance during the course of αMS or PA catalytic conversion.

Table 1. Relative Deviations (%) between γ Values of Pure H_2 and H_2+Kerosene (vapor) for γ Ranging Between 10^{-1} and 10^{-4}

	Saturated with Kerosene				Partially Saturated with Kerosene			
γ_{H2}	10^{-1}	10^{-2}	10^{-3}	10^{-4}	10^{-1}	10^{-2}	10^{-3}	10^{-4}
Peak	1.5	27.7	172.2	290.1	0.4	7.4	50.7	85.4
Averaged over 1 cm	1.6	16.2	74.2	95.7	0.5	4.5	21.1	27.6
Averaged over 4 cm	0.7	4.8	19.5	24.9	0.2	1.3	5.5	7.1

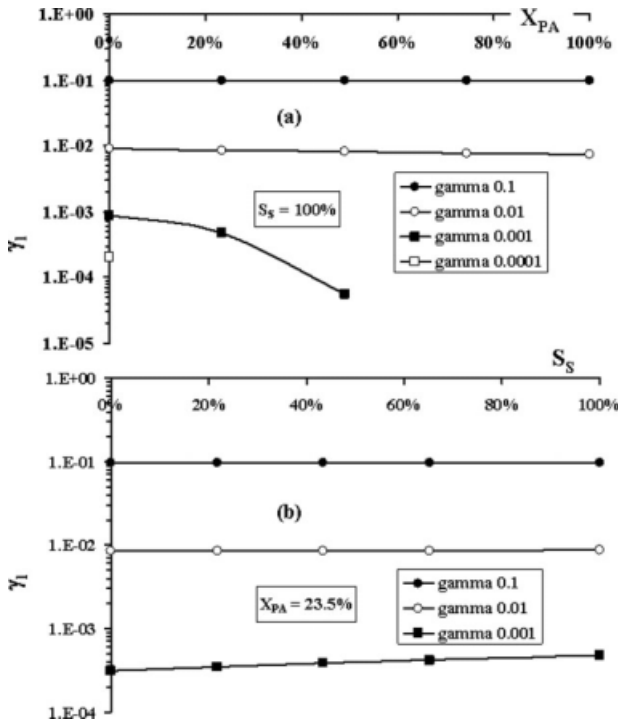

Figure 7. Evolution of liquid-phase gravitational amplification factor as a function of phenylacethylene conversion, X_{PA}, and (a) styrene selectivity, S_S, (b) for phenylacetylene/kerosene-H_2 system.

Starting values at $X_{PA} = 0$: $MPPG_A = 441$ T^2/m : peak $\gamma_l = 10^{-1}$; $MPPG_A = 485$ T^2/m : peak $\gamma_l = 10^{-2}$; $MPPG_A = 489$ T^2/m : peak $\gamma_l = 10^{-3}$; $MPPG_A = 489.3$ T^2/m : peak $\gamma_l = 10^{-4}$.

Let us first assess the incidence of temperature on γ_g. The 0.16 M αMS/kerosene/H_2 system is considered and the average conversion rate of αMS, $dX_{\alpha MS}/dt$, and the average temperature rise, dT/dt is estimated (see Appendix B for model derivation and calculation details). The reactor model was solved in pseudo-steady state assuming adiabatic (reactor + liquid recycling loop) system across a 1-cm high catalyst layer. The initial conditions are changed after each pass through the reactor. It was found that $dX_{\alpha MS}/dt = 0.23\%$/min and $dT/dt = 0.03$ K/min. This source heating rate is too low beside the actual reactor is not adiabatic so that heat losses in the loop largely offset temperature surge above room temperature. In the current conditions, the isothermal hypothesis is largely verified and so does γ_g invariance.

To assess the incidence of compositional changes on γ_l, Figure 7 depicts the evolution of the liquid-phase gravitational amplification factor of the 0.15 M PA/kerosene/H_2 system as a function of phenylacetylene conversion X_{PA} (Figure 7a) at 100% styrene selectivity, S_S, and as a function of S_S (Figure 7b) at $X_{PA} = 23.5\%$. The liquid mixture mass magnetic susceptibility, to be used in Eq. 1, is estimated as a function of X_{PA} and S_S using an additive law similar to Eq. 19. The mass magnetic susceptibilities of kerosene, phenylacetylene (PA), styrene (S), ethylbenzene (EB) and *n*-decane (internal standard) are estimated to be, respectively, $-2.56\cdot10^{-8}$ m^3/kg, $-6.12\cdot10^{-9}$ m^3/kg, $-8.23\cdot10^{-9}$ m^3/kg, $-9.11\cdot10^{-9}$ m^3/kg and $-1.06\cdot10^{-8}$ m^3/kg.[40] The starting composition ($X_{PA} = 0$) allowed to achieve peak γ_l values equal 10^{-1} at $MPPG_A = 441$ T^2/m, 10^{-2} at $MPPG_A = 485$ T^2/m, 10^{-3} at $MPPG_A = 489$ T^2/m and 10^{-4} at $MPPG_A = 489.3$ T^2/m. As can be seen from Figure 7, it is not feasible to maintain μ-gravity conditions for $\gamma_l < 10^{-2}$ with X_{PA} in excess of about 25%. For example, after $X_{PA} = 25\%$ at $S_S = 100\%$, γ_l becomes negative and both **[C^1]** and **[C^2]** are violated. At lower PA conversions, say $X_{PA} < 25\%$, μ-gravity levels down to 10^{-3} are achievable regardless of selectivity. In conservative terms, however, it could be stated that conditions **[C^1]** and **[C^2]** could easily be fulfilled for γ_l down to 10^{-2} regardless of reaction conversion and selectivity.

Recap of salient features

- In spite of the 2D nature of the magnetic field, scaling gravity amplification factors, γ, based solely on axial component B_z, as in Eq. 1, is an acceptable approximation.
- Magnetic fields up to 10 Tesla are virtually effectless on thermodynamic equilibria and diffusional fluxes so that classical thermodynamic calculations remain valid. In hydrogenating systems, because of H_2 smallest molar weight, solvent evaporation must be accounted for in matching between gas and liquid mass magnetic susceptibilities.
- Temperature variations affect (diamagnetic) gas mass magnetic susceptibility whereas (diamagnetic) liquid mass susceptibility is sensitive to the species distribution as evolved by the reaction. For hydrogenation systems, it is conservative to assume magnetic mimicry for γ between 1 and 10^{-2} regardless of conversion or selectivity levels. Accomplishment of deeper μ-gravity levels would require estimation of ad hoc limit conversion levels above which changes in mixture mass magnetic susceptibilities cannot be ignored.
- It is possible to achieve acceptable degrees of axial homogeneity for γ between 1 and 10^{-2} up to 1-cm bed heights. The magnet maximum field of 9 T is not a bottleneck as γ peaks down to 10^{-4} are attainable with 489.4 T^2/m (Figure 6b) which is well below the 650 T^2/m limit of current magnet (Figure 1b). Future improvements concern better winding strategies of NbTi coil to enlarge further the homogeneity domain. As far as organic liquids and diamagnetic gases are concerned, there is prospect for lunar- and Mars-like gravity catalytic tests in multiphase reactors to well be emulated on Earth using strong inhomogeneous magnetic fields.

Experimental Results and Discussion

μ-Gravity using paramagnetic gas and liquid

Figures 8a–c illustrate comparisons between liquid holdups, wetting efficiencies and two-phase pressure drops for $\gamma_l = \gamma_g = 1$ (Earth conditions, magnetic field disabled) and for $\gamma_l \approx \gamma_g \approx 0.42$ (nearly Martian conditions, magnetic field enabled) in a mini-trickle bed packed with 1-mm glass beads. To achieve nearly Mars gravity in the bed, the paramagnetic air/34.5% w/w aqueous $MnCl_2$ two-phase flow system was subjected to a peak gradient of -26.33 T^2/m. As can be seen, the liquid magnetic force oriented upwardly contributes to amplify liquid holdup in μ-gravity conditions.

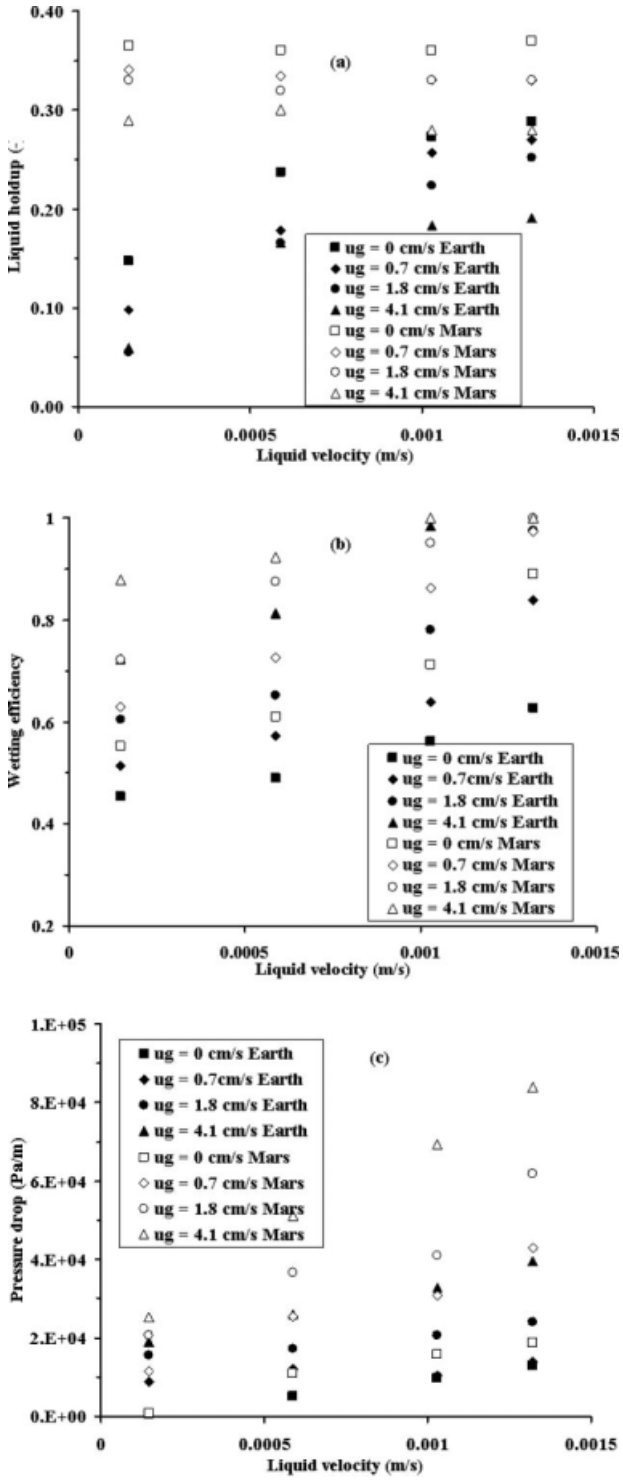

Figure 8. Comparative evolutions of liquid holdup (a), wetting efficiency (b) and two-phase pressure drop (c) for Earth operation vs. nearly-Mars gravity conditions of a two-phase flow of a paramagnetic gas–paramagnetic liquid system in a trickle bed reactor.

Air/aqueous $MnCl_2$ 34.5% (w/w) system, $MPPG_{A'} = -26.33$ T^2/m, 1-mm glass beads.

For liquid single-phase flow ($u_g = 0$ m/s) when the magnetic field is enabled, liquid holdup monopolizes almost the whole bed porous volume even at low liquid superficial velocity (u_l). In addition, it is less sensitive towards liquid velocity. Such a propensity to bed flooding can be ascribed to a tangible reduction in liquid gravitational driving force. In two-phase flow ($u_g \neq 0$ and μ-gravity conditions, liquid holdup exhibits the classical decreasing trend with increasing gas superficial velocity. Figure 8a indicates that under Martian gravity, and for the same reason as the $u_g = 0$ m/s case, liquid holdup values would be higher then on Earth by about a factor two, everything else being kept identical. It is plausible that though trickle flow regime prevails in terrene conditions for the selected gas and liquid velocities, this is no longer sustainable in reduced gravity conditions where the higher liquid holdups measured lean more in favor of a bubbling or pulsing flow regime. This would be coherent with the parabolic-flight tests at $\gamma = 10^{-2}$ carried out on trickle beds by Motil et al.[11] in which it was shown that trickle flow regime was unstable and was supplanted by a bubbly or a pulsing flow.

A comparison between wetting efficiencies on Earth and in Mars conditions for down-flow mode is illustrated in Figure 8b. The liquid magnetization force density amounting to -8875 N/m^3, largely outweighs its gas counterpart (-8 N/m^3) and dictates through liquid holdup increase in hypogravity a direct action on the wetting efficiency augmentation. In addition to an increase in wetting efficiency with gas and liquid superficial velocities (Figure 8b), it is worthy of notice that a reduction in γ values also occasions a surge in wetting efficiency. This is due to the fact that the liquid velocities chosen in the study were purposely too small to realize all the time partial-wetting reminiscent of trickle flow regime. Any attempt at correlating wetting efficiency and liquid holdup in non-terrene conditions requires re-engineering classical trickle bed correlations by handling the additional variability stemming from the gravity factor. It is interesting to note that despite liquid holdup in Mars conditions is very high does not mean that the whole packing is wet as revealed by the improved tendency of wetting efficiency with increasing gas and liquid superficial velocities. Such improvement in wetting efficiency ranges in reduced gravity from 30% at $u_G = 0$ to 12% at the highest gas velocity (Figure 8b).

A comparison between two-phase pressure drops on Earth and for Mars gravity conditions in down-flow mode is shown in Figure 8c. Two-phase pressure drops exhibit monotonic increases with gas and liquid superficial velocities, whether for Earth or Mars conditions. However, two-phase pressure drops are higher in reduced gravity with soaring values the higher the gas velocities. The ratio of hydrostatic heads on Mars and Earth $(\rho_l \varepsilon_l \gamma_l g)_{Mars}/(\rho_l \varepsilon_l g)_{Earth}$ being close to 1 in our conditions is worthy of notice. This means that the higher pressure drops recorded in Mars conditions cannot be imputed to hydrostatic head effects alone but that friction forces must likely undergo some changes because of a shift in flow patterns from trickle flow to presumably pulse/bubbly regimes. It is likely that because of the higher liquid holdups in Mars conditions, the gas flow experiences more resistance to protrude throughout the bed so that the gas-liquid frictions are significant and differ from those at work in

conventional trickle flow regime. In this way, both gas-liquid and liquid-solid contacting are likely to improve through reduced γ_l (and γ_g) and thus particles surface wetted by the liquid increases as shown in Figure 8b.

In terms of modeling pressure gradient in trickle-bed reactors in reduced gravity, it would likely be insufficient just to content with crushing the value of the gravity constant in the momentum balance equations, and significant efforts have to be devoted to formulate appropriate drag closures valid in contexts with likely bubbly or pulsing flows. This interpretation aligns with Motil et al.[11] findings regarding access to genuine frictional pressure drops, which can be approached more accurately under microgravity conditions, in addition to the fact that it is much higher than that for single-phase flow liquid only.

For illustration, let us take a naïve up-scaling of the well-known slit model[51] in which the gas-liquid interfacial interactions are dropped because of the very low gas (few cm/s) and liquid superficial (about 1 mm/s) velocities involved under 1*g* experiments. A steady-state unidirectional fully developed and fully wetted bed formulation can be cast in which the gravitational acceleration g is symbolically replaced by its reduced gravity value γ_l (or γ_g) $\times$ g. Considering the very low magnetic susceptibility values in play, magnetization-induced field effects can be ignored. It is relatively easy to arrive at the following modified slit model for μ-gravity contexts:

$$-\frac{dP}{dz}\frac{1}{\rho_g \gamma_g g}+1=\left(\frac{\varepsilon}{\varepsilon_g}\right)^3\left(E_1\frac{\mathrm{Re}_g}{\mathrm{Ga}_g}+E_2\frac{\mathrm{Re}_g^2}{\mathrm{Ga}_g}\right) \tag{20}$$

$$-\frac{dP}{dz}\frac{1}{\rho_l \gamma_l g}+1=\left(\frac{\varepsilon}{\varepsilon_l}\right)^3\left(E_1\frac{\mathrm{Re}_l}{\mathrm{Ga}_l}+E_2\frac{\mathrm{Re}_l^2}{\mathrm{Ga}_l}\right) \tag{21}$$

Similarly, Motil et al.[11] two-phase pressure drop correlation developed for reduced gravity contexts is:

$$-\frac{\Delta P}{H}\frac{d_p}{\rho_l u_l^2}\frac{\varepsilon^3}{1-\varepsilon}=1.8+\frac{1-\varepsilon}{\mathrm{Re}'_l}\left(180+0.8\sqrt{\frac{\mathrm{Re}'_g}{1-\varepsilon}}\left(\frac{\mathrm{Su}_l(1-\varepsilon)}{\mathrm{Re}'_l}\right)^{2/3}\right) \tag{22}$$

In which:

$$\mathrm{Ga}_\alpha=\frac{\rho_\alpha^2\gamma_\alpha g d_p^3\varepsilon^3}{\eta_\alpha^2(1-\varepsilon)^3};\ \mathrm{Re}_\alpha=\frac{\rho_\alpha d_p u_\alpha}{\eta_\alpha(1-\varepsilon)};\ \gamma_\alpha=\left(1+\frac{\hat{\chi}_\alpha}{g\mu_o}B_z\frac{\partial B_z}{\partial z}\right)$$

$$\text{and}\ \mathrm{Re}'_\alpha=\frac{\rho_\alpha d_p u_\alpha}{\eta_\alpha}\ \text{and}\ \mathrm{Su}_l=\frac{\rho_l\sigma_l d_p}{\eta_l^2}$$

Figure 9 shows the simulated behavior regarding two-phase pressure gradients for air/water system flowing in a trickle bed subject to microgravity of 10^{-2} based on correlated data of Motil et al.[11] and on a reduced-gravity amended slit model for trickle flow (Eqs. 20 and 21). The first stemming result is that pressure drop in reduced gravity is higher than the one predicted using trickle flow models

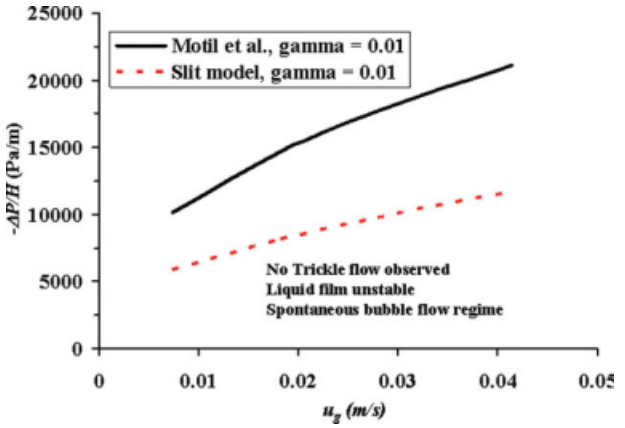

Figure 9. Pressure drop comparisons between slit model[51] and Motil et al.[11] correlation for microgravity conditions in a trickle bed with 1-mm glass beads and u_l = 1.5 mm/s.

[Color figure can be viewed in the online issue, which is available at www.interscience.wiley.com.]

and would indirectly provide theoretical basis for the results shown in Figure 8c. The second element concerns the fact that no matter if the Galileo number for the gas phase accounts for reduced gravity (see Galileo number above), it seems the gas-liquid drag force closure used in the slit model would be inadequate for predicting the boosted up pressure drops in reduced gravity. The third point questions the validity of Ergun-like derivations for the drag force closures in structurally separated gas-liquid flows as in trickle flow and their extension for reduced gravity flow structures that do not necessarily bear the same flow patterns (e.g., bubbly flow and pulse flow regimes).

μ-Gravity using diamagnetic gas and liquid

Hydrodynamics. Figures 10a,b illustrate comparisons between liquid holdups and wetting efficiencies for $\gamma_l = \gamma_g = 1$ (Earth conditions, magnetic field disabled) and for peak values of $\gamma_l \approx \gamma_g$ covering the range $[10^{-1}{:}10^{-4}]$ in the case of α-methylstyrene/kerosene-hydrogen system. Different values of maximum magnetic fields were required to reach a maximum product between magnetic field intensity and magnetic field gradient ranging from 440 to 489.4 T^2/m around point A (Figure 2b) where the mini-trickle bed reactor was positioned.

In general, regardless of the prevailing reduced gravity conditions, liquid holdup increases with increased liquid velocity and decreases with increased gas velocity. As the results show also, liquid holdup increases with increasing $B_z\partial B_z/\partial z$ (or decreasing γ values) because the resistance to liquid flow increases strongly due to liquid magnetization force. A peak value of $B_z\partial B_z/\partial z$ of 440 T^2/m provides hypogravity conditions with a gravitational amplification factor of $10^{-1} \pm 20\%$ along the 1-cm bed height as discussed from Figure 4. The magnetic body forces are orientated upwards for both liquid and gas thus partially counterbalancing the fluids' weights. This yields longer residence time for the liquid phase with, as a main result, an increase in liquid volume held in the bed. Similar arguments hold also for the

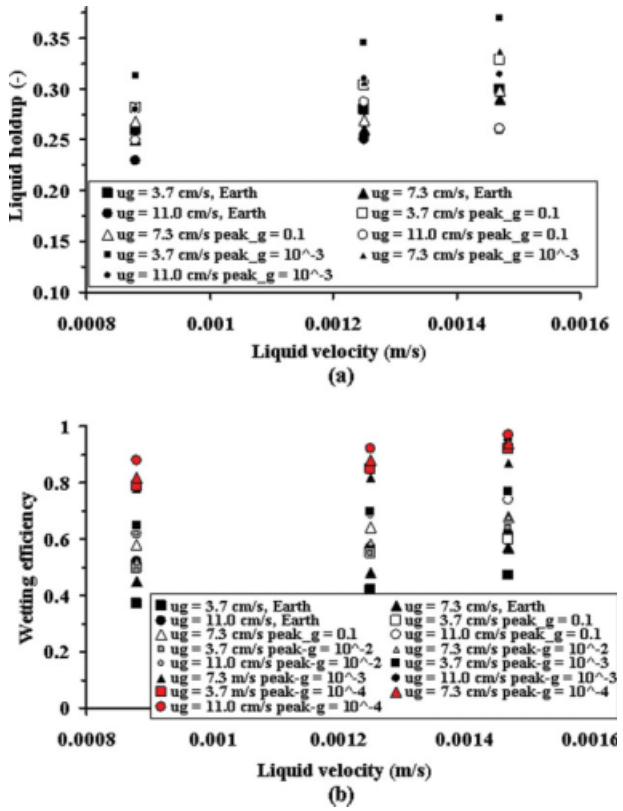

Figure 10. Comparative evolutions of liquid holdup (a) and wetting efficiency (b) at various gas and liquid superficial velocities for Earth operation vs. μ-gravity conditions of a two-phase flow of a diamagnetic gas–diamagnetic liquid system in a trickle bed reactor.

αMS/kerosene-H_2 system, peak values $\gamma_g \approx \gamma_l = 10^{-1}$, 10^{-2}, 10^{-3}, and 10^{-4}. [Color figure can be viewed in the online issue, which is available at www.interscience.wiley.com.]

488.6 T^2/m product gradient yielding a peak gravitational amplification factor of 10^{-3}. However, according to Figure 4 calculations and in spite of the liquid holdup yet increasing, it is unrealistic to assume a representative γ value as low as 10^{-3} for the whole bed considering the very large gradients in γ taking place over very small distances.

In the absence of magnetic field, the wetting efficiency increases as expected as both gas and/or liquid velocity increase (Figure 10b). As liquid velocity increases, wetting efficiency improves further due to an increase in liquid holdup (Figure 10a). Wetting efficiency average improvement is about 5% for each liquid velocity increment. Also, improvement in wetting efficiency is contributed through improved liquid contacting over the packing area as a result of increasing gas-liquid interfacial shear stress by means of increased gas velocity. This yields about 7% gain in wetting efficiency for each gas velocity increment.

When the magnetic field is enabled, an analogous tendency was observed and the effect was an increase in wetting efficiency with gas and liquid velocities in agreement with $B = 0$ case. It was shown that magnetically-emulated μ-gravity increases liquid holdup. An immediate consequence to liquid holdup improvement is a better wetting efficiency. Wetting efficiency is thus increasing progressively with increasing $B_z\partial B_z/\partial z$ (or decreasing γ values) through a knock-down of liquid gravitational driving force in the bed. The trends for both wetting efficiency and liquid holdup already depicted above in the case of the paramagnetic gas–paramagnetic liquid systems appear thus to be also valid for the diamagnetic gas–diamagnetic liquid systems.

Reaction Data. To identify the limiting reactant, the diffusion fluxes of the two reactants should be compared. The ratio $\Gamma_R = D_{eL}C_{Li}/b(D_{eG}C_G)$ is indicative of the relative availability of the species at the reaction site. Thus, a value of $\Gamma_R \gg 1$ implies gaseous reactant limitations, while Γ_R [dlt] 1 indicates liquid-reactant limitations.[52] For our systems, Γ_R was near 0.92 and the reaction was considered as being slightly liquid-reactant limited. This means that it is possible to evaluate the wetting efficiency changes in terms of conversion of the limiting liquid reactant.

Figure 11a shows αMS experimental conversion results. In the absence of magnetic field, αMS conversion, $X_{\alpha MS}$, to

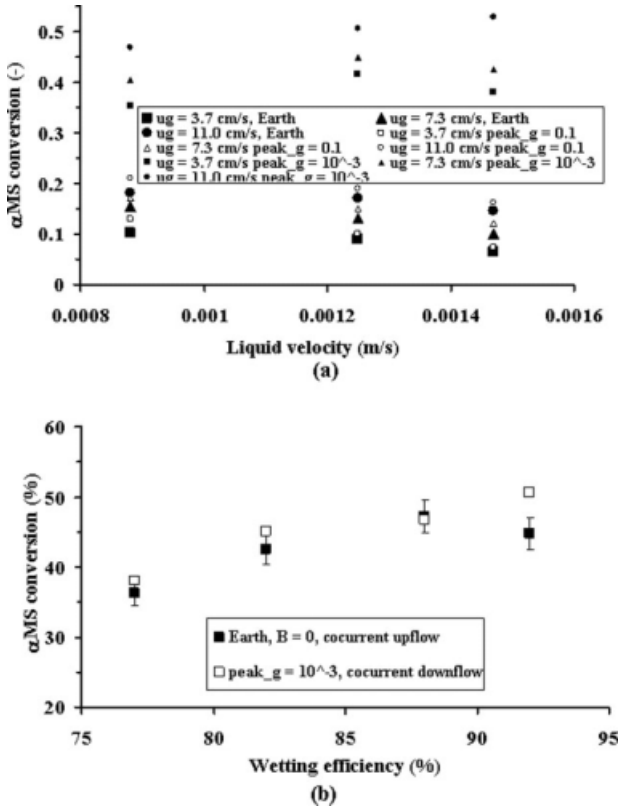

Figure 11. Comparative evolutions of αMS conversion (a) and styrene selectivity (b) at various gas and liquid superficial velocities for Earth operation vs. μ-gravity conditions of a two-phase flow of a diamagnetic gas–diamagnetic liquid system in a trickle bed reactor.

αMS/kerosene-H_2 system and phenylacethylene/kerosene-H_2 system, peak values $\gamma_g \approx \gamma_l = 10^{-1}$, 10^{-2}, 10^{-3}, and 10^{-4}.

cumene increases with gas velocity from 10% for the lowest to 19% for the highest velocity. This increase is due to increasing wetting efficiencies as shown in Figure 10b if $\Gamma_R = 0.92$ is hypothesized to be sufficient to highlight the sensitivity of conversion to the liquid reactant deficit. The conversion variation as a function of liquid velocity follows a decreasing trend as a likely result of a reduction in liquid residence time with increased liquid superficial velocity. A slight decrease, about 4–5%, is observed for conversions for any given gas velocity when liquid velocity is being increased.

The first value of the product between magnetic field intensity and magnetic field gradient used in the experiment was 440 T^2/m ensuring $\gamma = 10^{-1}$ in the catalyst bed. The experimental results indicate an increase in conversion by 2–3% comparatively with $B = 0$-case conversion. An explanation for this tiny rise is provided by the slight improvement in wetting efficiency from $\gamma = 1$ down to $\gamma = 10^{-1}$, everything else being invariant. This increase in wetting efficiency under magnetic field tends to ameliorate conversion for a liquid-reactant limited reaction as a result of more access through the catalyst surface of liquid αMS.

The gain in conversion is even more spectacular at 488.6 T^2/m for which the attained peak γ is 10^{-3}, Figure 11a. αMS conversion is increasing by a factor 3 for the same gas and liquid superficial velocities, giving considerable process intensification. It was calculated that $MPPG_A = 488.6$ T^2/m product gradient generates an average gravitational amplification factor value of 0.147 around a peak gravitational amplification factor value of 10^{-3}. Therefore an improved liquid distribution and better accessibility to catalyst sites in reduced gravity could be an interesting process intensification asset and further understanding of the nature of liquid flow structure in these conditions is required.

Let us examine to what extent the magnetic field effects on αMS conversion is ascribable *exclusively* to hydrodynamic origins. Figure 11b shows αMS conversion as a function of wetting efficiency when the magnetic field is disabled for a co-current *upflow* mode, and when the magnetic field is enabled for the co-current down-flow operation mode. The peak gravitational amplification factor value is 10^{-3} and its average value is 0.146 across the 1-cm catalyst bed. Normally, provided the magnetic field changes neither the reaction chemistry nor its pathway and has no function other than controlling wetting efficiency and liquid holdup via hydrodynamic levers (Kelvin force), identical αMS conversions should be obtained under equal wetting efficiency and contact time between catalyst and liquid, and this regardless of the prevailing magnetic field. In an upflow mode, wetting efficiency is higher then in down-flow mode resulting in better liquid-reactant conversions for liquid-limited reactions. Conversion data were thus obtained in upflow mode (Figure 11b). Then conversion measurements were realized in down-flow after enabling the magnetic field that realizes the same wetting efficiency and liquid contact time as in upflow mode at $B = 0$. Figure 11b demonstrates beyond doubt that the function of the magnetic field is hydrodynamic and consists in mainly an improvement of wetting efficiency in the down-flow mode. Dissimilarities between experimental points are small and the assumption that the magnetic field acts only hydrodynamically proves true.

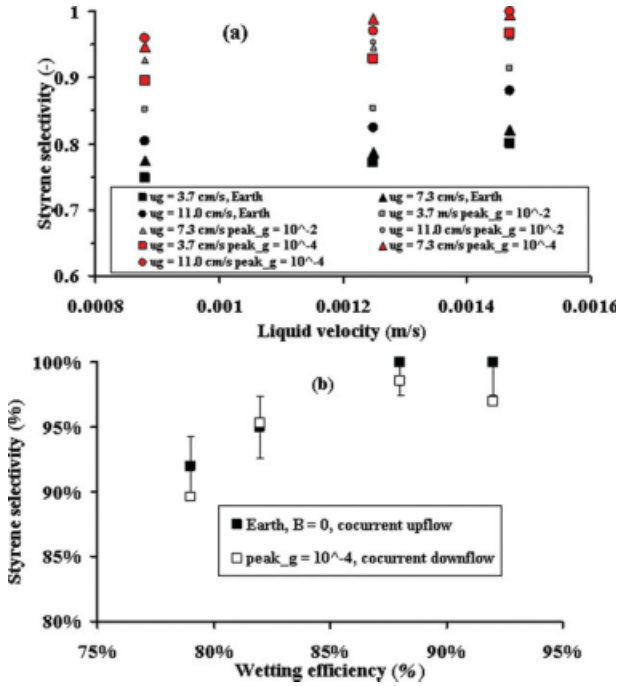

Figure 12. Commutation of magnetization force into artificial gravity force.

Comparisons of αMS conversion (a) in trickle bed at peak $\gamma_g \approx \gamma_l = 10^{-3}$ and of styrene selectivity (b) in trickle bed at peak $\gamma_g \approx \gamma_l = 10^{-4}$ with corresponding conversion and selectivity in co-current upflow bed in Earth conditions ($B = 0$) at iso-space-time and iso-wetting efficiency. [Color figure can be viewed in the online issue, which is available at www.interscience.wiley.com.]

Figure 12a shows the experimental styrene selectivity results, S_S, in trickle bed mode. Following the same arguments regarding the interrelation between magnetic field, wetting efficiency and phenylacetylene hydrogenation, it is possible to interpret the increasing trend of styrene selectivity with wetting efficiency along the same line developed for αMS hydrogenation. Figure 12b shows S_S as a function of wetting efficiency when the magnetic field is disabled in co-current upflow mode and when the magnetic field is enabled for co-current down-flow operation mode ($\gamma = 10^{-4}$) while equal wetting efficiencies are being achieved as explained earlier. The peak gravitational amplification factor value is 10^{-4} and the average value is 0.145. Imposing the same wetting efficiency yields equal styrene selectivities as shown in the figure. As for the αMS conversion case, dissimilarities between experimental points are small and the hypothesis that the magnetic field operates only at a hydrodynamic level is accurate.

Concluding Remarks

A new method was developed to obtain artificial μ-gravity in a controlled laboratory facility capable of providing simulated lunar/Martian gravity or microgravity environments for experiments on passive/reactive multiphase flows. Its applicability was illustrated in the case of miniature trickle beds, loaded with inert and catalytic particles, where flowing gas

and liquid would feel artificial μ-gravity inside the atmospheric bore of a superconducting magnet. The magnet generates large magnetic field strengths and magnetic field gradients to compensate for gravity. Magnetic mimicry of artificial gravity is realized by commuting into apparent gravity acceleration the magnetization force at work on both diamagnetic and paramagnetic non-magnetic and electrically non-conducting fluids. The scaling property to be maintained invariant in multiphase systems to achieve magnetic mimicry is phasic mass magnetic susceptibility.

The following factors were analyzed in terms of their repercussions on the spatial homogeneity of μ-gravity: axial vs. radial/azimuthal Kelvin magnetic force components and spatial distribution of magnetic field inside the magnet, incidence of magnetic fields on gas solubility, solvent evaporation and diffusion, and finally the effects of temperature and conversion of catalytic reaction on the change in mass magnetic susceptibilities.

Hydrodynamic measurements (liquid holdup, wetting efficiency, pressure drop) were realized for both gas paramagnetic–liquid paramagnetic and gas diamagnetic–liquid diamagnetic systems. Conversion and selectivity data were also measured with and without magnetic fields at constant wetting efficiency and contact time. It was shown that magnetic fields affect conversion and selectivity of catalytic reactions exclusively via hydrodynamic phenomena (mainly wetting efficiency). It was found that magnetic fields affect neither the reaction chemistry nor its pathway which otherwise would have jeopardized through epiphenomenal magnetically-induced effects the analogy between artificial gravity produced by strong inhomogeneous magnetic fields and actual μ-gravity in space or in non-terrene conditions.

The experimental system consisted of a miniature packed-bed reactor that was sufficiently small to fit within the atmospheric bore of the magnetic field setup. Considering the space and weight constraints of spatial flights, reactor scale-up, in the conventional assertion, is not an issue as relatively small-sized reactors using catalyst particles of similar size, as those tested in the miniature bed, are to be devised to fit within the space shuttles. For instance, provided similar catalyst particle sizes are used, reactor scale-up and hydrodynamics (for instance, wetting efficiency and liquid holdup) would remain indifferent to the capillary forces relative to gravity.

Acknowledgements

Financial support from the Natural Sciences and Engineering Research Council of Canada is gratefully acknowledged.

Notation

$\underline{\mathbf{B}}$ = magnetic induction field vector, T
C_i = i-species mole concentration, mol/m^3
D = reactor diameter, cm
D_i = molecular diffusion coefficient, m^2/s
$\underline{\mathbf{E}}$ = electric field vector, V/m
$\underline{\mathbf{F}}_{\mathrm{L}\alpha}$ = α-phase Lorentz magnetohydrodynamic body force density, N/m^3
$\underline{\mathbf{F}}_{\mathrm{M}\alpha}$ = α-phase Kelvin body force density, N/m^3
f_i^{α} = α-phase i-species fugacity, -
g = earth gravity acceleration, m/s^2
K_{H} = Henry's constant, Pa
$k_{\mathrm{g}}a$ = volumetric gas-side mass transfer coefficient, s^{-1}
J_i = i-species total mole flux, mol/(m^2·s)
L = reactor length, cm
M_i = molar weight, kg/mol
T = temperature, K or °
P = pressure, atm
R = ideal gas law constant, J/mol/K
u_{α} = α-phase superficial velocity, m/s
$\overline{v}_i^{\alpha}$ = α-phase i-species partial molar volume, m^3/mol
w_i = i-species mass fraction, -
x_i = liquid-phase mole fraction, -
y_i = gas-phase mole fraction, -
z = axial coordinate, cm
ε_{α} = α-phase holdup per unit reactor volume, -
γ_{α} = α-phase gravitational amplification factor, -
μ_0 = vacuum permeability, $4\pi \times 10^{-7}$ N/A^2
$\overline{\mu}_i$ = i-species magneto-chemical potential, J/mol
ρ_{α} = α-phase density kg/m^3
σ_{α} = α-phase electrical conductivity, Ω^{-1}m^{-1}
χ_{α} = α-phase volumetric magnetic susceptibility, -
χ_i^{α} = α-phase i-species volumetric magnetic susceptibility, -
$\hat{\chi}_{\alpha}$ = α-phase mass magnetic susceptibility, -

Subscripts/Superscripts

0,o = without magnetic field
g = gas
l = liquid
m = molar basis
r = radial
z = axial
θ = azimuthal

Acronyms

αMS = α-methylstyrene
C = cumene
EB = ethylbenzene
MPPG = maximum (minimum) peak product gradient
PA = phenylacetylene
ROI = region of interest
S = styrene

Literature Cited

1. Pletser V. Short duration microgravity experiments in physical and life sciences during parabolic flights: the first 30 ESA campaigns. *Acta Astronautica*. 2004;55:829–854.
2. Tsujino T. Trends in research on the utilization of microgravity—competition and collaboration between research in space and research on the ground. *Quarterly Rev*. 2006;21:89–105.
3. Advanced life support project plan, Crew and thermal systems division, Lyndon B. Johnson space center, National aeronautics and space administration, Houston, Texas, CTSD-ADV-348-REV C, *JSC 39168* 2002:1–41.
4. Nashashibi-Rabah M, Christodoulatos C, Korfiatis GP. Development of a gravity-independent wastewater bioprocessor for advanced life support in space. *Water Environment Res*. 2005;77:138–145.
5. Sornchamni T, Atwater JE, Akse JR, Wheeler RR Jr, Jovanovic GN. Magnetically assisted filtration for solid waste separation and concentration in microgravity and hypogravity. *Ind Eng Chem Res*. 2005;44:9199–9207.
6. Ostrach S. Low-gravity fluid flows. *Ann Rev Fluid Mech*. 1982;14:313–345.
7. Motil BJ, Singh BS. NASA's microgravity fluid physics strategic research roadmap. *42nd AIAA Aerospace Sciences Meeting and Exhibit*,123, 2004.
8. Drysdale AE, Ewert MK, Hanford AJ. Life support approaches for Mars missions. *Adv Space Res*. 2003;31:51–61.
9. Srydhar KR, Finn JE, Kliss MH. In-situ resource utilization technologies for Mars life support systems. *Adv Space Res*. 2002;25:249–255.
10. Motil BJ, Nahra HK, Balakotaiah V. Hydrodynamics of packed bed reactor in low gravity. *NASA/TM - 2005–213806*, 2005.
11. Motil BJ, Balakotaiah V, Kamotani Y. Gas-liquid two-phase flow through packed beds in microgravity. *AIChE J*. 2003;49:557–565.

12. Beaugnon E, Tournier R. Levitation of organic materials. *Nature*. 1991;349:470.
13. Wakayama NI, Zhong C, Kiyoshi T, Itoh K, Wada H. Control of vertical acceleration (effective gravity) between normal and microgravity. *AIChE J*. 2001;47:2640–2643.
14. Tagawa T, Ozoe H, Inoue K, Ito M, Sassa K, Asai S. Transient characteristics of convection and diffusion of oxygen gas in an open vertical cylinder under magnetizing and gravitational forces. *Chem Eng Sci*. 2001;56:4217–4223.
15. Wang LB, Wakayama NI. Control of natural convection in non- and low-conducting diamagnetic fluids in a cubical enclosure using inhomogeneous magnetic fields with different directions. *Chem Eng Sci*. 2002;57:1867–1876.
16. Lin SX, Zhou M, Azzi A, Xu GJ, Wakayama NI, Ataka M. Magnet used for protein crystallization: novel attempts to improve the crystal quality. *Biochem Biophys Res Commun*. 2000;275:274–284.
17. Munteanu MC, Iliuta I, Larachi F. Process intensification in artificial gravity. *Ind Eng Chem Res*. 2005;44:9384–9390.
18. Rinaldi C, Zahn M. Effects of spin viscosity on ferrofluids flow profiles in alternating and rotating magnetic fields. *Phys Fluids*. 2002;14:2847–2870.
19. Rinaldi C, Brenner H. Body versus surface forces in continuum mechanics: is the Maxwell stress tensor a physically objective Cauchy stress? *Phys Rev E*. 2002;65:036615.
20. Ikezoe Y, Hirota N, Nakagawa J, Kitazawa K. Making water levitate. *Nature*. 1998;393:749–750.
21. Beaugnon E, Tournier R. Levitation of water and organic-substances in high static magnetic-fields. *J Phys III France*. 1991;1:1423–1428.
22. Paine CG, Seidel GM. Magnetic-levitation of condensed hydrogen. *Rev Sci Instrum*. 1991;62:3022–3024.
23. Berry MV, Geim AK. Of flying frogs and levitrons. *Eur J Phys*. 1997;18:307–313.
24. Davidson PA. *An Introduction to Magnetohydrodynamics*, United Kindgom: Cambridge University Press, 2001.
25. Turek F, Lange R. Mass transfer in trickle-bed reactors at low Reynolds number. *Chem Eng Sci*. 1981;36:569–579.
26. Germain A, Lefebvre A, L'Homme GA. Experimental study of a catalytic trickle-bed reactor. *Adv Chem*. 1974;133:164–180.
27. Herskowitz M, Carbonell RG, Smith JM. Effectiveness factors and mass-transfer in trickle-bed reactors. *AIChE J*. 1979;25:272–283.
28. Meille V, de Bellefon C, Schweich D. Kinetics of α-methylstyrene hydrogenation over Pd/Al_2O_3. *Ind Eng Chem Res*. 2002;41:1711–1715.
29. Meille V, de Bellefon C. Effect of water on α-methylstyrene hydrogenation on Pd/Al_2O_3. *Can J Chem Eng*. 2004;82:190–193.
30. Visser JBM, Stankiewicz A, van Dierendonck LL, Manna L, Sicardi S, Baldi G. Dynamic operation of a 3-phase upflow reactor for the hydrogenation of phenylacetylene. *Catal Today*. 1994;20:485–500.
31. Wilhite BA, Wu R, Huang X, McCready MJ, Varma A. Enhancing performance of three-phase catalytic packed-bed reactors. *AIChE J*. 2001;47:2548–2556.
32. Wilhite BA, Huang X, McCready MJ, Varma A. Effects of induced pulsing flow on trickle-bed reactor performance. *Ind Eng Chem Res*. 2002;42:2139–2145.
33. Wilhite BA, McCready MJ, Varma A. Kinetics of phenylacetylene hydrogenation over $Pt/\gamma\text{-}Al_2O_3$ catalyst. *Ind Eng Chem Res*. 2002;41:3345–3350.
34. Huang X, Wilhite BA, McCready MJ, Varma A. Phenylacetylene hydrogenation in a three-phase catalytic packed-bed reactor: experiments and model. *Chem Eng Sci*. 2003;58:3465–3471.
35. Lazzaroni CL, Keselman HR, Figoli NS. Colorimetric evaluation of the efficiency of liquid-solid contacting in trickle flow. *Ind Eng Chem Res*. 1988;27:1132–1135.
36. Vignaud A, Maitre X, Guillot G, Durand E, de Rochefort L, Robert P, Vives V, Santus R, Darrasse L. Magnetic susceptibility matching at the air-tissue interface in rat lung by using a superparamagnetic intravascular contrast agent: influence on transverse relaxation time of hyperpolarized helium-3. *Magn Reson Med*. 2005;54:28–33.
37. Ludovisi D, Cha SS, Ramachandran N, Worek WM. Effect of magnetic field on two-layered natural/thermocapillary convection. *Int Commun Heat Mass Transfer*. 2007;34:523–533.
38. Cañas-Marin WA, Ortiz-Arango JD, Guerrero-Aconcha UE, Lira-Galeana C. Thermodynamics of wax precipitation under the influence of magnetic fields. *AIChE J*. 2006;52:2887–2897.
39. Herskowitz M, Wisniak J, Skiadman L. Hydrogen solubility in organic liquids. *J Chem Eng Data*. 1983;28:164–166.
40. *Handbook of Chemistry and Physics*, 83rd ed. Section 3—*Physical Constants of Organic Compounds*,CRC Press LLC, 2003.
41. Marano JJ, Holder GD. Characterization of Fischer-Tropsch liquid for vapor-liquid equilibria calculations. *Fluid Phase Equilibria*. 1997;138:1–21.
42. Sandler SI. *Chemical and Engineering Thermodynamics*, 3rd ed. New York: Wiley, 1999.
43. Chartier P, Gross M, Spiegler KS. *Applications de la thermodynamique du non-équilibre, Bases d'énergétique pratique*, Ed. France: Hermann, 1975.
44. Mulay LN. *Magnetic Susceptibility*. New York: John Wiley, 1963.
45. Kuchel PW, Chapman BE, Bubb WA, Hansen PE, Durrant CJ, Hertzberg MP. Magnetic susceptibility: solutions, emulsions, and cells. *Concepts Magn Reson*. 2003;18A:56–71.
46. Yaici W, Laurent A, Midoux N, Charpentier JC. Determination of gas-side mass transfer coefficients in trickle-bed reactors in the presence of an aqueous or an organic liquid phase. *Int Chem Eng*. 1988;28:299–305.
47. Goto S, Levec J, Smith JM. Mass transfer in packed beds with two-phase flow. *Ind Eng Chem Process Des Dev*. 1975;14:473–478.
48. Reiss LP. Cocurrent gas-liquid contacting in packed columns. *Ind Eng Chem Process Des Dev*. 1967;6:486–499.
49. Fukushima S, Kusaka K. Boundary of hydrodynamic flow region and gas-phase mass-transfer coefficient in packed column with cocurrent downward flow. *J Chem Eng Jpn*. 1978;11:241–244.
50. du Trémolet de Lacheisserie E. *Magnétisme. I—Fondements*, vol. 1, Collection Grenoble Sciences, Les Ulis cedex A, France: EDP Sciences, 2000.
51. Holub RA, Dudukovic MP, Ramachandran PA. Pressure drop, liquid holdup, and flow regime transition in trickle flow. *AIChE J*. 1993; 39:302–321.
52. Khadilkar MR, Wu YX, Al-Dahhan MH, Dudukovic MP, Colakyan M. Comparison of trickle-bed and upflow reactor performance at high pressure: model predictions and experimental observations. *Chem Eng Sci*. 1996;51:2139–2148.

Appendix A

Henry's law constant K_H of H_2 in kerosene is based on the work of Herskowitz et al.[39] At $T = 298.1$ K and $P = 1$ atm, $K_H = 3.25 \cdot 10^8$ Pa. Kerosene vapor pressure, $P_2^v = 133.3$ Pa in the same conditions.

Hydrogen volumetric magnetic susceptibility in the gas phase $\chi_1^g = -2.05 \cdot 10^{-9}$, whereas H_2 volume magnetic susceptibility in the liquid phase ($\chi_1^l = -2.42 \cdot 10^{-6}$) was calculated as[40]:

$$\chi_1^l = \frac{\rho_1^l}{M_1} \chi_{m1}^l \tag{A1}$$

where ρ_1^l is H_2 liquid density (= 70.8 kg/m^3), M_1 is H_2 molar mass and χ_{ml}^l liquid molar magnetic susceptibility (=$6.83 \cdot 10^{-11}$ m^3/mol).[40]

Hydrogen partial molar volume in kerosene, $\overline{v}_1^l$ (=$15.67 \cdot 10^{-6}$ m^3/mol), was estimated according to Marano and Holder method, considering n-C_{14} as kerosene proxy.[41] Kerosene partial molar volume in liquid phase was estimated to be $\overline{v}_1^2 = 2.16 \cdot 10^{-4}$ m^3/mol.

Kerosene vapor volumetric magnetic susceptibility ($\chi_2{}^g = -1.44 \cdot 10^{-7}$) was approximated assuming the mass magnetic susceptibility to be phase-indifferent:

$$\chi_2^g = \frac{\rho_2^g}{\rho_2^l} \chi_2^l \tag{A2}$$

where χ_2^l is the kerosene liquid volume magnetic susceptibility (= $-2.02 \cdot 10^{-5}$), ρ_2^l is the kerosene liquid density (= 790 kg/m^3) and ρ_2^g the kerosene vapor density (= 5.64 kg/m^3).

Appendix B

To describe αMS hydrogenation kinetics, a Langmuir-Hinshelwood rate law developed by Turek and Lange was used[25]:

$$\Re = \frac{k\,K_{\alpha MS}\,C_{\alpha MS}\,C_{H_2}}{1 + K_{\alpha MS}\,C_{\alpha MS}} \tag{B1}$$

where k is a surface-reaction rate constant and $K_{\alpha\mathrm{MS}}$ is the adsorption equilibrium constant for αMS:

$$k = k_0\, e^{-E/RT} \tag{B2}$$

$$K_{\alpha MS} = K_{0\alpha MS}\, e^{-\Delta H_r/RT} \tag{B3}$$

The energy and mass balance equations assuming full wetting in the catalytic layer and reactor plug flow in both gas and liquid for αMS, cumene (C) and hydrogen, are as follows:

$$\left(u_l c_{p,l}\rho_l + u_g c_{p,H_2}\rho_{H_2}\right)\frac{\mathrm{d}T}{\mathrm{d}Z} = -\Delta H_r\,\rho_p(1-\varepsilon)\Re; \qquad T\big|_{z=0,t=0} = 298\mathrm{K} \tag{B4}$$

$$-u_l\frac{\mathrm{d}C_{\alpha MS}}{\mathrm{d}z} = \rho_p(1-\varepsilon)\Re \tag{B5}$$

$$-u_l\frac{\mathrm{d}C_{H_2,l}}{\mathrm{d}z} = \rho_p(1-\varepsilon)\Re - k_l a\left(\frac{P}{He} - C_{H_2,l}\right); \qquad C_{H_2,l}\big|_{z=0,t=0} = 0 \tag{B6}$$

$$u_l\frac{\mathrm{d}C_C}{\mathrm{d}z} = \rho_p(1-\varepsilon)\Re \quad ; C_C\big|_{z=0,t=0} = 0 \tag{B7}$$

The range of operating variables under reaction conditions and the constants are given in Table B.1.

Table B.1. Operating conditions and constants for the heat up 0.16 M αMS/kerosene/H_2 system

ΔH_r, kJ/mol	−111.2
E, J/mol	$38.7\cdot10^3$
$C_{p,l}$, kJ/kg·K	2.0
C_p,$H2$, kJ/kg·K	14.30
k_0, m^3/kg·s	10.7
P, atm	1
u_l, mm/S	1.25
u_g,cm/S	3.67
ρ_p, kg/m^3	2583
ε, m^3/m^3	0.37
$K_{0\alpha MS}$, m^3/kmol	$4.2\cdot10^{-3}$
K_H, atm·m^3/kmol	387.6
$k_l a$, S^{-1}	0.02
$MPPG_A$, T^2/m	488.6

Manuscript received May 15, 2008, and revision received Oct. 10, 2008.